Check for updates

The Higgs boson couplings: past, present, and future. The relationships between Higgs boson and other known particles as measured by current and future experiments

Giacomo Ortona*

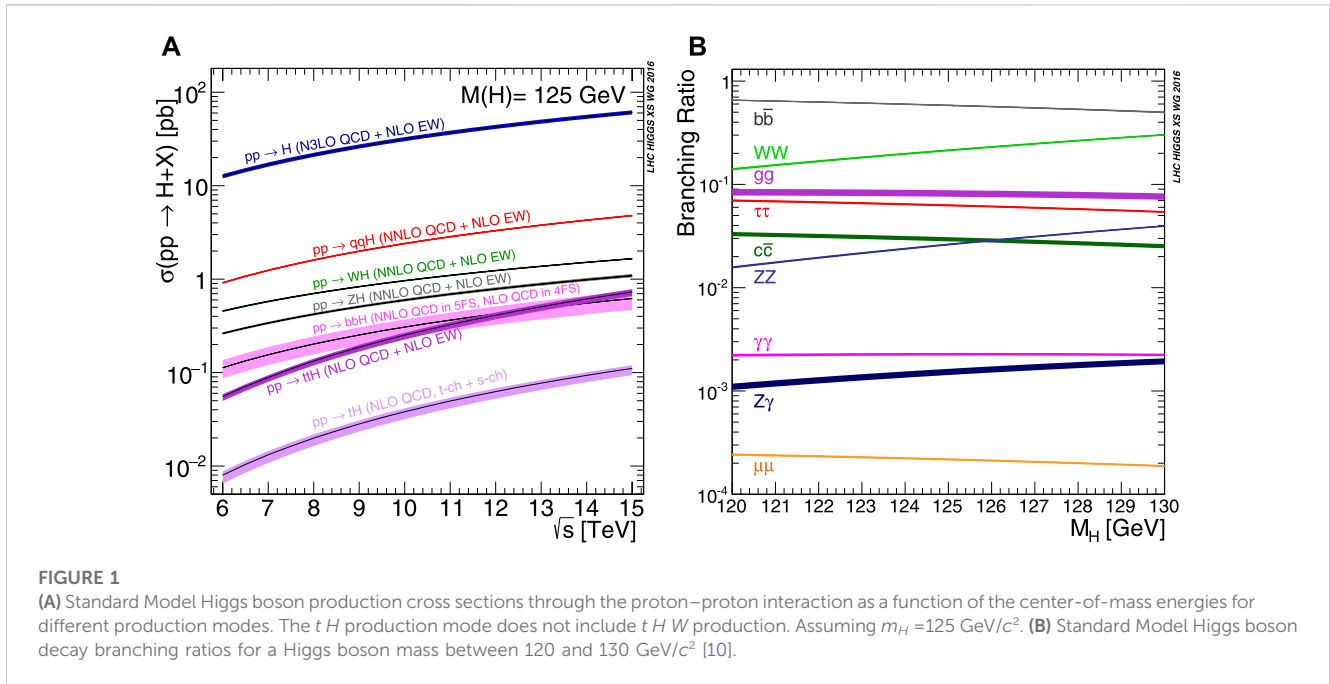Istituto Nazionale di Fisica Nucleare (INFN), Sezione di Torino, Torino, Italy

The discovery of the Higgs boson, a fundamental particle of the Standard Model, at the Large Hadron Collider (LHC) in 2012, marked a monumental milestone in the field of particle physics. Since then, extensive research has been conducted to understand the properties and interactions of the Higgs boson, particularly its couplings with other known particles. This article provides a review of the past, present, and future measurements of the Higgs boson couplings, with a focus on the most recent experimental developments. It discusses the experimental techniques and methods used to study the Higgs boson couplings, including the production and decay channels employed in various experiments. The article highlights the important relationships between the Higgs boson and other known particles, including the gauge bosons (W and Z bosons), quarks, and leptons and the Higgs boson itself, through its self-interaction. After discussing the channels used by ATLAS and CMS collaborations to measure the Higgs boson coupling to the other standard model particles, the article will present an overview of the latest results obtained at the LHC, commenting on how various measurements have evolved over time along with a better comprehension of the detectors and ever more refined analysis techniques. Future collider developments and expectation for the measurement of the Higgs boson couplings and double-Higgs boson production with increased precision and accuracy will be discussed along with the main challenges faced by future experiments.

KEYWORDS

Higgs-boson, EWSB, LHC, CMS, ATLAS, frontiers

1 Introduction

The Standard Model (SM) of particle physics is one of the most successful scientific theories ever developed, with confirmed predictions spanning many orders of magnitude at great precision, and the Higgs boson plays a pivotal role in it. According to the SM, as particles interact with the Higgs field, they acquire mass through a mechanism called electroweak symmetry breaking (EWSB). The Higgs boson is the quantum excitation associated with fluctuations in the Higgs field, and its presence is a necessary consequence of this mechanism. The Higgs boson is, therefore, essential for explaining

FIGURE 1
(A) Standard Model Higgs boson production cross sections through the proton–proton interaction as a function of the center-of-mass energies for different production modes. The *t H* production mode does not include *t H W* production. Assuming m_H =125 GeV/c^2. **(B)** Standard Model Higgs boson decay branching ratios for a Higgs boson mass between 120 and 130 GeV/c^2 [10].

the origin of mass and maintaining the internal consistency of the theory, and its existence was one of the most important predictions of the theory.

Given its importance in the SM, one of the main goals of the CERN Large Hadron Collider (LHC) was indeed to produce, observe, and study the Higgs boson. The LHC started colliding protons in 2010, for the first period of data collection at a center of mass energy of $\sqrt{s}$ = 7 TeV until 2012, when the energy in the center of mass was increased to 8 TeV for 1 year. This period is known as Run 1. After a shutdown period dedicated to upgrades and maintenance, the LHC Run 2 ran from 2015 to 2018 at an energy of 13 TeV. After another shutdown period, Run 3 started in 2022 at $\sqrt{s}$ = 13.6 TeV. The task of discovery and studying the Higgs boson is performed by the ATLAS [1] and CMS [2] experiments and collaborations; two large multipurpose experiments developed mainly to study proton–proton collisions at the LHC. So far, the LHC has delivered to the CMS (ATLAS) experiment 29 fb⁻¹ (28 fb⁻¹), 163 fb⁻¹ (157 fb⁻¹), and 50 fb⁻¹ (48 fb⁻¹) in runs 1, 2, and 3, respectively, for a total of ∼ 243 fb⁻¹ (232 fb⁻¹). The experiments have been able to record more than 90% of the delivered luminosity [3–8]. It is important to mention that the increase in the center of mass energy and luminosity obtained throughout the years came along with an important increase in the amount of pile-up events for each collisions, from an average of 10 pile-up collision for event in 2010 up to an average of 46 (48) in Run 2 (Run 3). Much effort has been expended by the collaborations in order to keep or improve the detectors performances despite this larger background.
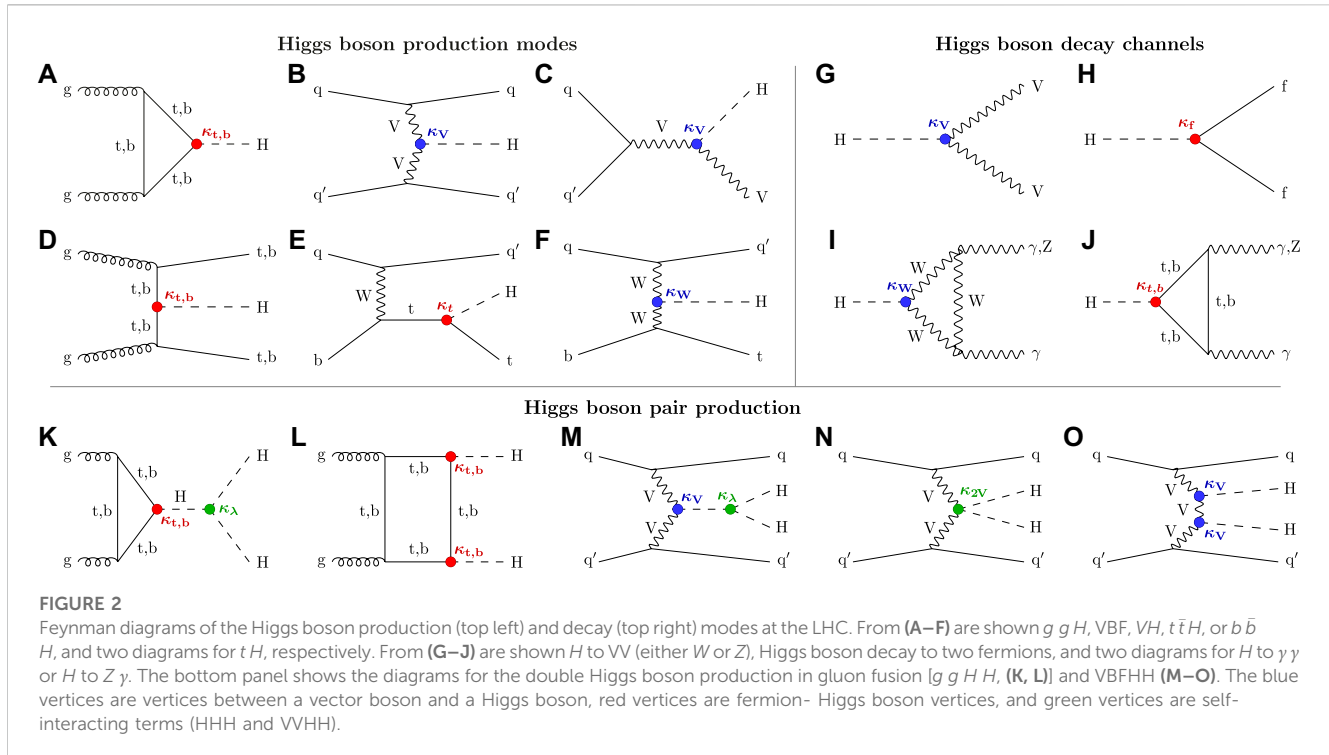
At hadron colliders, such as the LHC, the Higgs boson can be produced via several different mechanisms and can decay in several different final states. The cross sections (branching ratios) of the different production (decay) modes are shown in Figures 1A, B for a Higgs boson of about 125 GeV/c^2. The most common production mode is the gluon fusion (*g g H*) production, occurring when two gluons from the colliding protons interact by exchanging quarks. The quarks themselves can then emit a Higgs boson. A Feynman diagram

of this process is shown in Figure 2A [9]. This process has a cross section of 48.58 pb for a Higgs boson with a mass of 125 GeV/c^2 [10]. At 3.78 pb, the vector boson fusion (VBF) is more than 10 times rarer than *g g H*, but it is extremely relevant for the study of the Higgs boson coupling. In this process, as shown in Figure 2B, a pair of quarks from the two incoming protons exchange a vector boson (W or Z), emitting a Higgs boson in the process. Even rarer production modes are *VH* (Figure 2C, 2.25 pb), $t \bar{t} H$ and $b \bar{b} H$ (Figure 2D, 1 pb), and *t H* (Figures 2E, F, 0.07 pb). Even if rarer, these latest production modes can provide additional handles in the final state to separate the signal from the background and are, therefore, especially suited to address final states affected by a large background component.

The Higgs boson generated in the collision can then decay in several final states, as shown in Figures 2G–J. Decays to heavier particles (up to a pair of b-quarks) are generally preferred according to the SM. Thus, the generation of each Higgs boson in a proton–proton collision at the LHC involves its coupling to different SM particles, whether in production (quarks and vector bosons) or in decay (leptons, quarks, and vector bosons). Thanks to the small predicted width of the Higgs boson, the production and decay mechanism can be considered independent and can be factorized. The number of Higgs bosons produced in any given production (*ii*) and decay (*ff*) combination can, therefore, be computed according to the following formula:

$$N(ii \to H \to ff) \approx \sigma(ii \to H) \cdot B(H \to ff) = \sigma_i \times \text{B R}^f \approx \frac{\sigma_i \Gamma_f}{\Gamma_{\text{tot}}},$$

(1)

where Γ_f represents the partial decay width of the Higgs boson to a pair of f particles, and Γ_{tot} represents the total Higgs boson decay width. To simplify the notation, one can introduce the signal strength modifiers as $\mu_i^f = \frac{\sigma_i \times \text{BR}^f}{(\sigma_i \times \text{BR}^f)_{\text{SM}}}$, in order to parameterize eventual deviations from the SM. To disentangle effects in production and decay, for any particle j that couples in decay (production) with the Higgs boson, it is possible to define the

FIGURE 2
Feynman diagrams of the Higgs boson production (top left) and decay (top right) modes at the LHC. From **(A−F)** are shown ggH, VBF, VH, $t\bar{t}H$, or $b\bar{b}$ H, and two diagrams for tH, respectively. From **(G−J)** are shown H to VV (either W or Z), Higgs boson decay to two fermions, and two diagrams for H to $\gamma\gamma$ or H to $Z\gamma$. The bottom panel shows the diagrams for the double Higgs boson production in gluon fusion [$ggHH$, **(K, L)**] and VBFHH **(M−O)**. The blue vertices are vertices between a vector boson and a Higgs boson, red vertices are fermion- Higgs boson vertices, and green vertices are self-interacting terms (HHH and VVHH).

coupling modifier κ such that $\kappa_j^2 = \Gamma_j/\Gamma_j^{\text{SM}}$ for a Higgs boson decay and $\kappa_j^2 = \sigma_j/\sigma_j^{\text{SM}}$ in production. With this definition, also known as the κ-framework, the total Higgs boson width is thus $\Gamma_H = \frac{\kappa_H^2 \Gamma_H^{\text{SM}}}{1 - BR_H^{\text{SM}}}$ [11, 12]. In addition to the SM direct decays (vector bosons, leptons, and quarks), the κ_g and κ_γ couplings are also included to model the loop-mediated Higgs boson interaction with gluons and photons, respectively, without needing to resolve the loops. A convenient result of this notation is that, by definition, in the SM $\kappa_j = 1$ and $\mu_i^f = 1$ for all the allowed decays. Any significant deviation from unity would, therefore, indicate the presence of physics beyond the standard model (BSM).

This paper will focus on the determination of the k parameters. It is nevertheless important to mention that the high-energy physics community is exploring frameworks that are not only able to evaluate the (dis)agreement between the current results and the SM, such as with the signal strengths and the k-framework, but also to explore possible new physics signals hiding in the data collected by the ATLAS and CMS experiments. To this scope, the STXS [13] framework has been developed to provide a common definition for the measurements' phase space. This allows for an easier comparison between the experiment and the reinterpretation of the results within an effective field theory (EFT) framework.

Experimental signatures in the final states are exploited by the CMS and ATLAS collaborations in order to categorize the events according to their most likely production and decay mechanisms. Careful simulations of the experimental apparatus and precise predictions of the Higgs boson production cross sections [10] are used to predict the exact component, in terms of production processes, of each category, and with this knowledge, as we will discuss in the following sections, it is possible to perform a multidimensional statistical analysis to extract the couplings of the Higgs boson to each SM particle.

2 Measuring the Higgs couplings at the LHC

2.1 The Higgs coupling to bosons

Given its very short lifetime ($\tau_H \sim 1.58 \cdot 10^{-22}s$), experiments cannot directly observe the Higgs boson but must reconstruct it from its decay products. It is, thus, convenient to classify the observed events according to the particles involved in the Higgs boson decay and target each decay with a dedicated strategy.

The first very broad classification that can be made is whether the Higgs boson decays into a pair of bosons (W, Z, or photons via a quark loop) or into fermions (leptons and quarks). When it was first devised [14–19], the main goal of the EWSB mechanism was to provide mass to the weak interaction gauge bosons, i.e., W and Z, which was necessary to explain the short interaction range of the weak force. The measurement of the coupling of the Higgs boson to other gauge bosons is, therefore, a crucial test of the most fundamental aspects of the EWSB mechanism.

Experimentally, this is carried out at the LHC by measuring the Higgs boson decaying in pairs of bosons, either W^+W^- or ZZ. The final state where a Higgs boson decays into a pair of photon is also discussed in this section for convenience, although in the SM, the Higgs boson does not couple directly to massless photons, but can generate two photons in the final state via loops (Figures 2I, J).

2.1.1 Higgs to photons

The Higgs boson decay in a final state with two photons is among the most precise tools available to the experimental collaborations for assessing the properties of the Higgs boson, such as its mass and couplings. Due to the detector resolution effects, the distribution of the
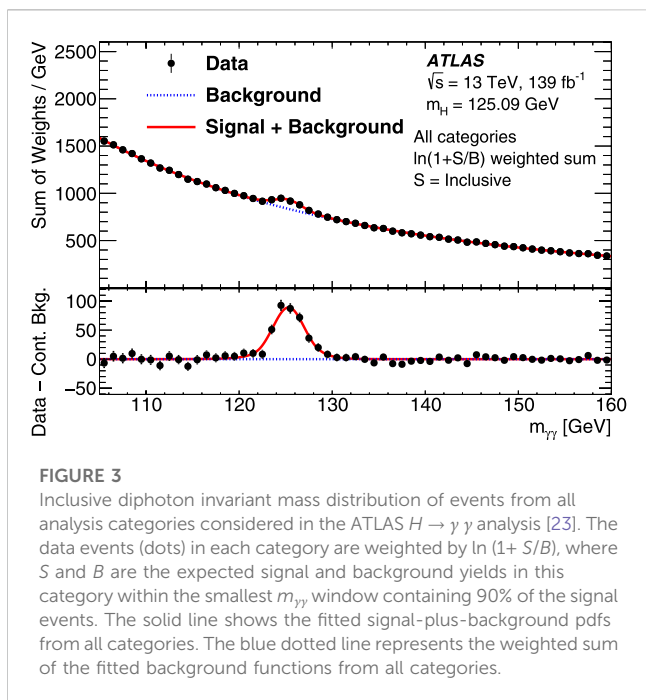
FIGURE 3

Inclusive diphoton invariant mass distribution of events from all analysis categories considered in the ATLAS $H \rightarrow \gamma\gamma$ analysis [23]. The data events (dots) in each category are weighted by ln (1+ S/B), where S and B are the expected signal and background yields in this category within the smallest $m_{\gamma\gamma}$ window containing 90% of the signal events. The solid line shows the fitted signal-plus-background pdfs from all categories. The blue dotted line represents the weighted sum of the fitted background functions from all categories.

invariant mass of the photon pair $m_{\gamma\gamma}$ shows a Gaussian-like peak centered at the Higgs boson mass over a falling combinatorial background due to the QCD production of two photons that follows a power-law distribution, as shown in Figure 3. The large number of events available in this channel allows measuring the properties of the signal peak with high precision. Multivariate analyses (MVAs) and machine learning techniques based on information related to photon quality, resolution, kinematics of the decay, and quality of the reconstructed system are used in order to classify events in different categories of signal-to-background ratio. In this way, the categories with low S/B will help constrain the background from the actual data, without having to rely on MC simulation. Although the strategy has remained the same, the increase in the number of collected events and a better understanding of the detectors obtained through years of data taking allowed the experiments to develop even more refined categorizations, from the original 5 (CMS) to 10 (ATLAS) used at the time of the discovery [20, 21] to the current 80 used in CMS or 101 used by ATLAS [22, 23], which are specifically designed to target the STXS measurement and are shown in Figure 4.

The main systematic uncertainties in the $H \rightarrow \gamma\gamma$ channel come from the uncertainties on the modeling of the background function and on photon measurement and identification. On the theory side, uncertainties on the renormalization and factorization scales and on the parton shower mechanism are also relevant, although overall statistical uncertainties still dominate this measurement.

2.1.2 Higgs to ZZ

Together with $H \rightarrow \gamma\gamma$, the ZZ decay channel of the Higgs boson was dubbed the *golden channel* due to its importance for the Higgs boson discovery and its precision, especially in the final state with four leptons (either muons or electrons). In the $H \rightarrow \gamma\gamma$ channel, there is an important number of signal events produced on top of a very large

combinatorial background; the situation is the opposite in the case of $H \rightarrow ZZ^{\star} \rightarrow 4\ell$. This is a relatively rare process, with a branching ratio of just 0.003% for a 125 GeV/c^2 Higgs boson. On the other hand, the presence of four well-identified leptons in the final state with the right masses and charges makes this a very clean channel, resulting in a large peak over a small and flat background in the invariant mass distribution of the four leptons and a very high signal-over-background ratio, as shown in Figure 5A.

The kinematics of the $H \rightarrow ZZ^{\star} \rightarrow 4\ell$ decay is fully described by the invariant mass of the four-lepton system, five of the decay angles, and the invariant masses of the two lepton pairs (m_{Z1}, m_{Z2}), as shown in Figure 5B. These variables hold a significant discriminant power to differentiate between the signal and background. Additional variables related to jets and extra leptons in the event can also be used to target specific production mechanisms. It is thus possible to achieve a large separation between the signal and background or between different signal hypotheses either by training machine learning algorithms on them [24] or by computing the ratio of the probabilities with a kinematic discriminant defined as follows: $K_D = \frac{P_{\text{sig}} (\vec{\Omega}^{H \rightarrow 4\ell} | m_{4\ell})}{P_{\text{sig}} (\vec{\Omega}^{H \rightarrow 4\ell} | m_{4\ell}) + P_{\text{bkg}} (\vec{\Omega}^{H \rightarrow 4\ell} | m_{4\ell})}$ [25, 26]. Dedicated kinematic discriminants can also be used to target specific decays, production modes, or BSM models.

Due to the low branching ratio of this channel, only the most common production modes were accessible to this channel in Run 1. CMS measured ggH and VBF [27], while ATLAS developed four categories, targeting VH as well [28]. Since then, thanks to the increase in the collected luminosity and to improvements in the analysis techniques, a more refined categorization was developed, with events classified in 12 categories targeting STXS1.1 by the ATLAS collaboration [24] and 22 categories closely following the STXS1.2 scheme [13] by the CMS collaboration [29]. This way, the two collaborations were able to measure the four main Higgs boson production modes (ggH, VBF, VH, and $t\bar{t}H$) with good precision.

The statistical uncertainty is still the largest component for the $H \rightarrow ZZ^{\star} \rightarrow 4\ell$ results, although in Run 2 is now very close to the systematic component. Among the main sources of systematic uncertainties, on the experimental side, there are uncertainties on lepton reconstruction and efficiency, and on the determination of the luminosity. The theoretical uncertainties are at least as important as the experimental uncertainties, with the most important uncertainties due to the QCD factorization and renormalization scales and uncertainties on the most important production modes' cross sections [24, 29].

The precision measurements in the $H \rightarrow ZZ$ decay channel are dominated by the 4ℓ final state, but it should be mentioned that the final states with two leptons and two neutrinos or two leptons and two jets are also investigated by the experimental collaborations, providing useful insights into the searches for anomalous couplings, off-shell ZZ production, or massive scalar resonances.

2.1.3 Higgs to WW

The $H \rightarrow WW$ channel is extremely sensitive for Higgs boson masses above the WW threshold of $\approx$160 GeV/c^2. For a mass of 125 GeV/c^2, its branching fraction is almost 10 times larger than that for $H \rightarrow ZZ$ and enjoys a relatively large signal-over-background
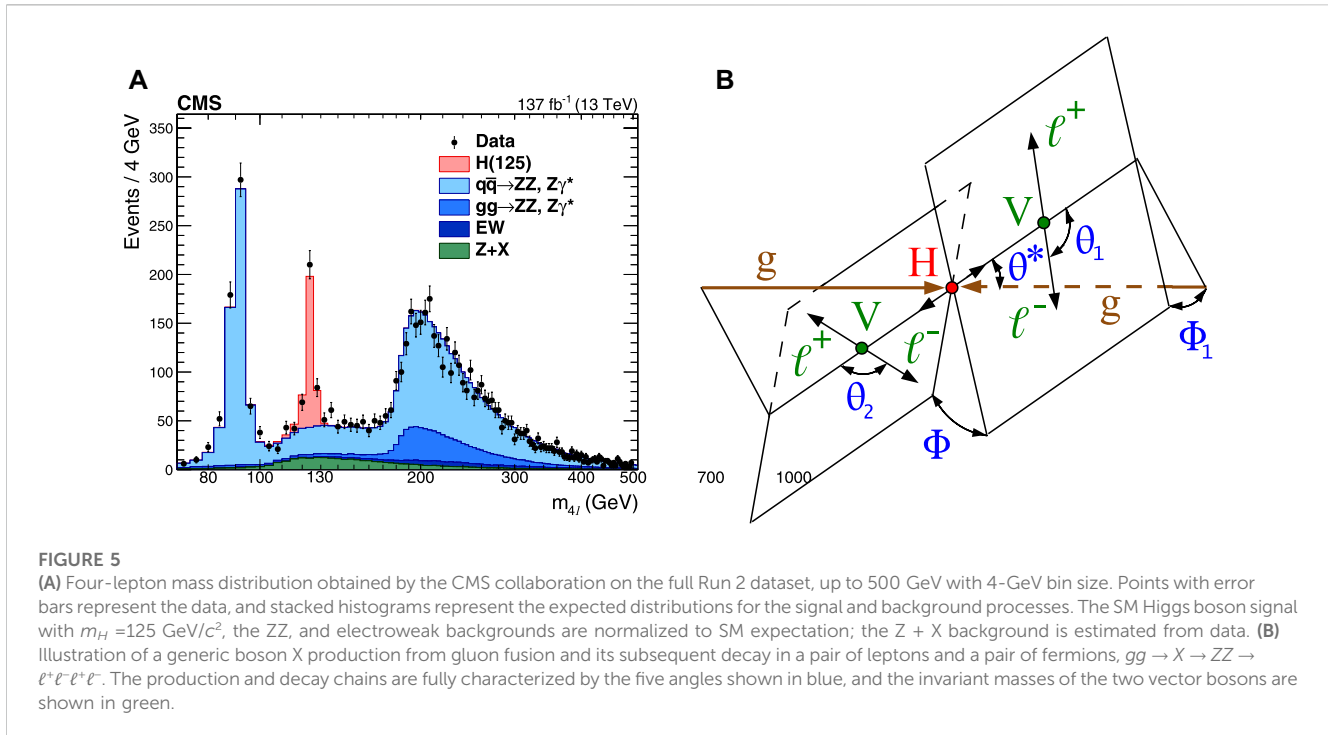
FIGURE 4
Contributions of STXS regions to the expected event yields in groups of analysis categories in the ATLAS $H \to \gamma\gamma$ analysis [23]. The vertical axis lists 28 merged STXS regions measured in the analysis, while the horizontal axis lists groups of analysis categories that target the same STXS region, weighted by their relative importance. Entries correspond to the percentage of the signal yield in each group of analysis categories (on the x-axis) that is contributed by a given STXS region (on the y-axis). Entries with a value below 1% are not shown.

FIGURE 5
(A) Four-lepton mass distribution obtained by the CMS collaboration on the full Run 2 dataset, up to 500 GeV with 4-GeV bin size. Points with error bars represent the data, and stacked histograms represent the expected distributions for the signal and background processes. The SM Higgs boson signal with m_H =125 GeV/c^2, the ZZ, and electroweak backgrounds are normalized to SM expectation; the Z + X background is estimated from data. **(B)** Illustration of a generic boson X production from gluon fusion and its subsequent decay in a pair of leptons and a pair of fermions, $gg \to X \to ZZ \to \ell^+\ell^-\ell^+\ell^-$. The production and decay chains are fully characterized by the five angles shown in blue, and the invariant masses of the two vector bosons are shown in green.

ratio. Despite this, the reconstruction of the W decay is experimentally much more challenging than the Z decay. The fully hadronic final state is affected by an overwhelming background at the LHC, so the most sensitive final state is the leptonic state, where the presence of two opposite sign leptons can be used to identify signal events with the discrimination being even more effective when both an electron and a muon are present in the final state ($H \to WW^* \to \mu\nu e\nu$). However, the W leptonic decays have undetectable neutrinos in the final state. The $H \to WW$ has, therefore. a worse mass resolution on the Higgs boson peak than the more precise $H \to ZZ^* \to 4\ell$ and $H \to \gamma\,\gamma$, resulting in a diminished sensitivity. The presence of neutrinos in the final state means that the analysis relies heavily on the reconstruction of missing energy in the analyzed event, under the assumption that most of that energy originates from the neutrinos produced in the W decay. To further complicate the analysis, there are many different background sources present in the final state, with the most important sources being non-resonant WW production, Drell–Yan, tW, and $t\bar{t}$ productions.

The large number of events allows separating them in several categories according to the transverse momentum p_T of the Higgs boson and extra objects in the events to distinguish between the $gg\,H$, and VBF, and, owing to the LHC Run 2, also the VH production mechanisms. The reconstructed invariant mass of the Higgs boson m_H is not a particularly discriminant variable for this decay due to its low resolution. The first instances of these analyses were, therefore, relying on variables with stronger discriminant power between the signal and background, such as the invariant mass of the visible leptons pair or the transverse mass $m_T = \sqrt{(E_T^{\ell\ell} + E_T^{\text{miss}})^2 - |p_T^{\ell\ell} + E_T^{\text{miss}}|^2}$. In the latest developments [30, 31], while these variables are still applied, they are used alongside machine learning techniques, especially deep neural network implementations that can profit from full information available in the event.

Systematic uncertainties mostly originate from theoretical uncertainties on the renormalization and factorization scales and, less importantly, from experimental uncertainties on lepton identification. The systematic uncertainties are the most relevant in the $gg\,H$ production mode, which is the most common process, providing a 10% uncertainty against a 6% statistical uncertainty. The statistical uncertainty is roughly at the same level as the systematic uncertainty in the VBF production mode and dominates the rarer VH production.

2.2 The Higgs coupling to fermions

In the SM, the Higgs boson couples to fermions through the Yukawa interaction. These couplings are generally more difficult to measure at the LHC than the bosonic ones. τ leptons present some unique challenges due to the presence of neutrinos and, in the case of their hadronic decays, jets in the final state. In the case of muons and electrons, their lighter masses result in very small branching ratios. In the case of quarks, they hadronize into jets and their identification is difficult against the large QCD background at the LHC. Nevertheless, the effort to measure the Yukawa couplings of the Higgs boson started as soon as the particle was discovered in 2012 with the third-generation particles (τ, t-quarks, and b-quarks) and it is now expanding to the second generation ($H \to \mu\,\mu$ and $H \to c\,\bar{c}$). Higgs boson couplings to electrons and lighter quarks are instead being tested in projections for future colliders.

2.2.1 Leptons: $H \to \tau\tau$

When considering all the possible decay modes of the τ lepton, the branching ratio of $H \to \tau\tau$ is about 6.3%, competitive or even

larger than bosonic channels. Nevertheless, this is somehow counterbalanced by a complex final state with the presence of neutrinos, light jets, or both. For this reasons, the actual observation of the Higgs boson decay in τ leptons was only achieved at the beginning of LHC Run 2 with the data collected in 2016 [32, 33]. Events are classified according to the different decays of the τ pair: $e\mu$, $\mu\mu$, $\mu\tau_h$, $e\tau_h$, and $\tau_h\tau_h$ and according to the number of jets in the event in order to boost sensitivity to production modes beyond gluon fusion. The ee final state is generally ignored as it is affected by a very large DY background and usually provides very little sensitivity. Much effort has been dedicated to improve the reconstruction and identification of the τ coming from the Higgs boson decays. This resulted in the development of likelihood-based estimators that greatly improved these searches [34, 35] and helped this channel to reach a sensitivity to the couplings close to that of the bosonic channels. This is especially true in subdominant production modes such as VBF, where the extra candle of the two jets from the VBF mechanism helps reduce the background, mostly DY, while at the same time profiting from the relative large branching ratio of this final state.

2.2.2 Leptons: $H \to \mu\mu$

At the face value, the strategy of the $H \to \mu\mu$ analysis looks relatively simple. The analysis is focused at the distribution of the reconstructed invariant mass of pairs of opposite-sign muons. The well-reconstructed $Z \to \mu\mu$ peak can be used to normalize the background component, and CMS and ATLAS excel in the reconstruction of muons. The main issue is given by the fact that the process is extremely rare with a branching ratio of just 0.02% on top of a large combinatorial background and with an S/B ratio of $\sim 1/1000$. Despite all these challenges, the CMS collaboration recently managed to obtain evidence [36] of this decay by profiting the whole LHC Run 2 luminosity, marking a very important milestone for the development of the Higgs studies at the LHC.

2.2.3 Bottom and charm

The Higgs boson decay into a pair of bottom quarks enjoys the largest decay branching ratio of the SM at 58.2% and a fair resolution on the Higgs boson peak of about 15%. The main challenge in measuring this decay is thus not the availability of candidates but, at first, separating jets originating from the decay of a b-quark from other jets originated from lighter quarks, and then further identifying which of those truly originate from a Higgs boson decay. This is one of the most important applications of machine learning techniques to high-energy physics. Several algorithms have been developed to this scope over the years, and some of them are now applied even when triggering on jets to quickly identify possible candidates. At the start of the LHC physics program, most of the effort was dedicated to identify b-jets coming from the main interaction vertex or from top quark decays. With the increase in energy and pile-up obtained between Run 1 and Run 2, these algorithms needed to be even more refined in order to keep up with the more challenging conditions. An illustration of these

algorithms' capabilities is shown in Figure 6A from the CMS collaboration. Since the larger amount of data in Run 2 now allows the collaboration to target the Higgs boson decay to charm quarks, the latest developments of these algorithms are focusing on developing neural networks [37, 38] that are able to separate not only heavy from light flavors but also c-quarks from b-quarks [39, 40], as shown in Figure 6B. ATLAS has shown a light (charm) jets rejection power of 600 (11) for a 70% efficiency in identifying b-jets and a rejection power of 70 for light jets and 9 for b-jets at a 30% efficiency on c-tagged jets [40]. CMS rejection power is 500 at 70% b-jet efficiency and approximately 40 for 30% efficiency on c-tagged jets [39, 41].

Armed with these tools, it is possible to tackle the measurement of the Higgs boson decay into b-quarks. Given the very large background of 2-jet events at the LHC, the observation was made possible in Run 2 by looking for events where the Higgs boson was produced in association with a vector boson [31, 42], where this measurement can provide a tight constraint on the Higgs boson couplings to vector bosons. By using the whole LHC Run 2 data and advanced machine learning techniques such as adversarial neural networks, it was finally possible to see evidence of VBF and ggH productions in this channel [43]. Another strategy to enhance the signal-over-background ratio is instead to look at highly boosted events, where the b-tagged jets are very collinear and almost merged together [44].

The search for the Higgs boson decay into a pair of c-quarks works similarly to the b-quarks but is made more challenging by a branching ratio 20 times smaller (2.9%), larger background, and c-jets that are harder to distinguish from the overwhelmingly large QCD background. Given these premises, it is hardly a surprise that this decay channel has not been observed yet. Nevertheless, the first promising results have been obtained with the Run 2 dataset in the $VH \to Vc\bar{c}$ channel [45, 46] and in the boosted jet topologies [47], suggesting that this measurement will be one of the most important results that will be explored in the upcoming LHC Run 3.

2.2.4 Top quark Yukawa

Among the couplings to different quark species, the top quark holds a special place. The top quark is the heaviest particle in the SM, and the top quark Yukawa coupling is, therefore, extremely important both for the stability of the SM and for the exploration of BSM models. Indeed, before the discovery of the Higgs boson in 2012, the best indirect estimate of its mass (at about 90 GeV/c^2) was obtained through global electro-weak fits, where among the most important components were the top quark and W masses [48]. Since the top quark is heavier than the Higgs boson, the $H \to t\bar{t}$ decay is not allowed, and the Higgs to top quark coupling must be measured either indirectly, by resolving the loop in the production and decay of the Higgs, or by measuring it from the production mechanism, such as $t\bar{t}H$ and tH. The first strategy would rely on assumptions on the relative composition of the loops and is a matter of interpretation of the available results. The latter is, therefore, the one most actively pursued at the experimental collaborations.

Whenever a sufficient amount of data are available, all the decay channels discussed so far try to develop categories especially
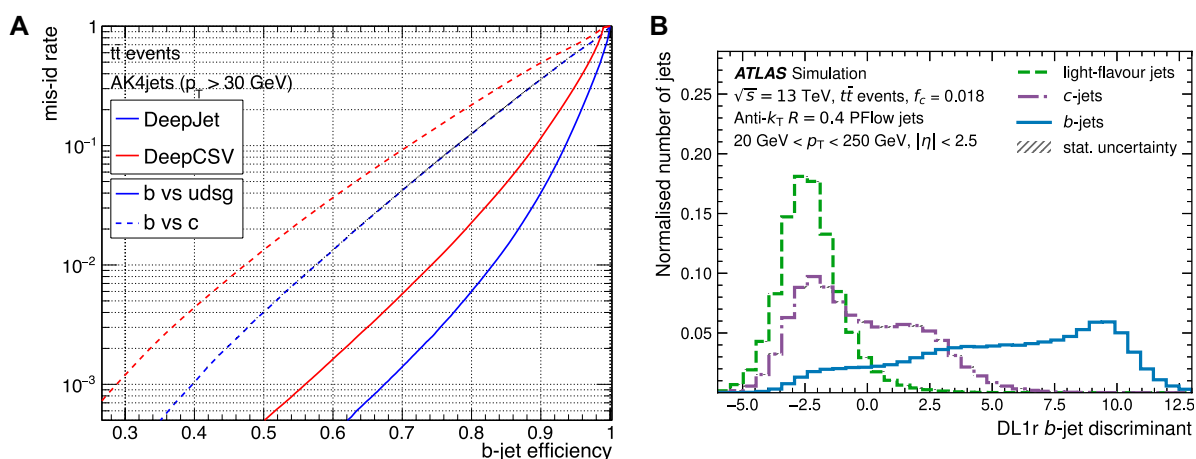
FIGURE 6
(A) B-tagging efficiency and misidentification rates for two different algorithms employed by the CMS collaboration. Both algorithms use a deep neural network to discriminate. Solid line: discrimination of b-quark jets against light (u, d, s, and (g) jets. Dashed line: b-quark jets against c jets. **(B)** Distribution of the deep learning DL1r algorithm by the ATLAS collaboration in differentiating between light (green), charm (purple), and bottom (blue) jets.

designed to target top quark associated production. In addition to the measurements from the different decay channels [49, 50], comprehensive analyses primarily dedicated to the measurement of the $t\bar{t}H$ and tH productions have also been prepared by the experiments [51]. They are designed to target final states with a different number of leptons (up to four), where leptons are either muons or electrons or taus that decay hadronically. In each category, the multiplicity of jets and b-tagged jets is then chosen accordingly to its compatibility with either the $t\bar{t}H$ or tH production. In this way, it is possible to target at the same moment the Higgs boson decay in WW, ZZ, and $\tau\tau$. State-of-the-art machine learning techniques are used both to separate the signal from the background and to separate $t\bar{t}H$ from tH events.

These analyses were able to observe the $t\bar{t}H$ production by themselves profiting of the full Run 2 data collection [49, 50] and provided the first hints of tH production.

3 Results from the LHC

Each of the decay channels discussed so far is sensitive only to those couplings that enter the Higgs boson production and the decay mode of that channel. The best way to assess the Higgs boson couplings in a comprehensive way is, therefore, to perform a combined measurement of all the channels together. This is a challenging task since one must take into account not only correlations between the Higgs boson couplings across different channels, whose determination is the goal of this exercise, but also among different background processes and systematic uncertainties. To avoid the possible double-counting effects, the final states should be mutually exclusive whenever possible. Excluding channels for which the actual sensitivity is too low to provide a meaningful constraint, such as $b\bar{b}H$, in the most general realization of the combined fit after the LHC Run 2, there are six production modes (ggH, VBF, WH, ZH, $t\bar{t}H$, and tH) and seven decay channels (ZZ, WW, $\gamma\gamma$, $\tau\tau$, bb, $\mu\mu$, and $Z\gamma$). It is useful to merge the $t\bar{t}H$ and tH

production modes as they are both dominated by κ_t, and the statistical significance of the tH production mode is still very low. Not all combinations of production and decay are actually accessible with the current datasets, so some of them are either neglected or merged in order to improve their significance. In total, CMS (ATLAS) identified 30 (25) production × decay unique categories. The information from these categories is combined to measure up to nine coupling modifiers: κ_Z, κ_W, κ_γ, κ_g, κ_t, κ_τ, κ_b, κ_μ, and $\kappa_{Z\gamma}$. Furthermore, extra couplings such as Higgs to invisible or to BSM particles can also be included in the fit. The measurement of κ_c is not included since it is not yet precise enough to contribute to the global fit but has been established by CMS to be in the range $1.1 < |\kappa_c| < 5.5$ [45] and by ATLAS in the range $|\kappa_c| < 8.5$ [46].

The procedure used to perform the combined fit and to estimate the parameters of interest was established by a common agreement before the Higgs boson discovery [52], and it is still used today. It is based on a profile likelihood technique with asymptotic approximation, where the systematic uncertainties are the nuisance parameters. The full correlation of the nuisance parameters across years and channels is taken into account when performing the fit, and systematic uncertainties are considered correlated when they are related to the same underlying effect. The fit is an extremely onerous and complex task. It includes $O(10^4)$ nuisance parameters for each experiment, and in the end is a summary of most of our knowledge of the Higgs boson. The results of the combined likelihood fit by the CMS collaboration [9, 53] are shown in Figure 7. The same results from the ATLAS collaboration are very similar [54]. It can be observed that the measurements obtained at the LHC are in remarkable agreement with the SM predictions. To appreciate the extent of the work performed in these years by the experimental collaborations, it is possible, for example, to look at the improvements obtained on the precision on some of these couplings, as shown in Figure 7B. At the discovery of the Higgs boson, even the couplings accessible to the most precise channels contributing to the discovery, such as κ_Z, κ_γ, κ_g, and κ_W, were measured with less than 50% accuracy. By the end
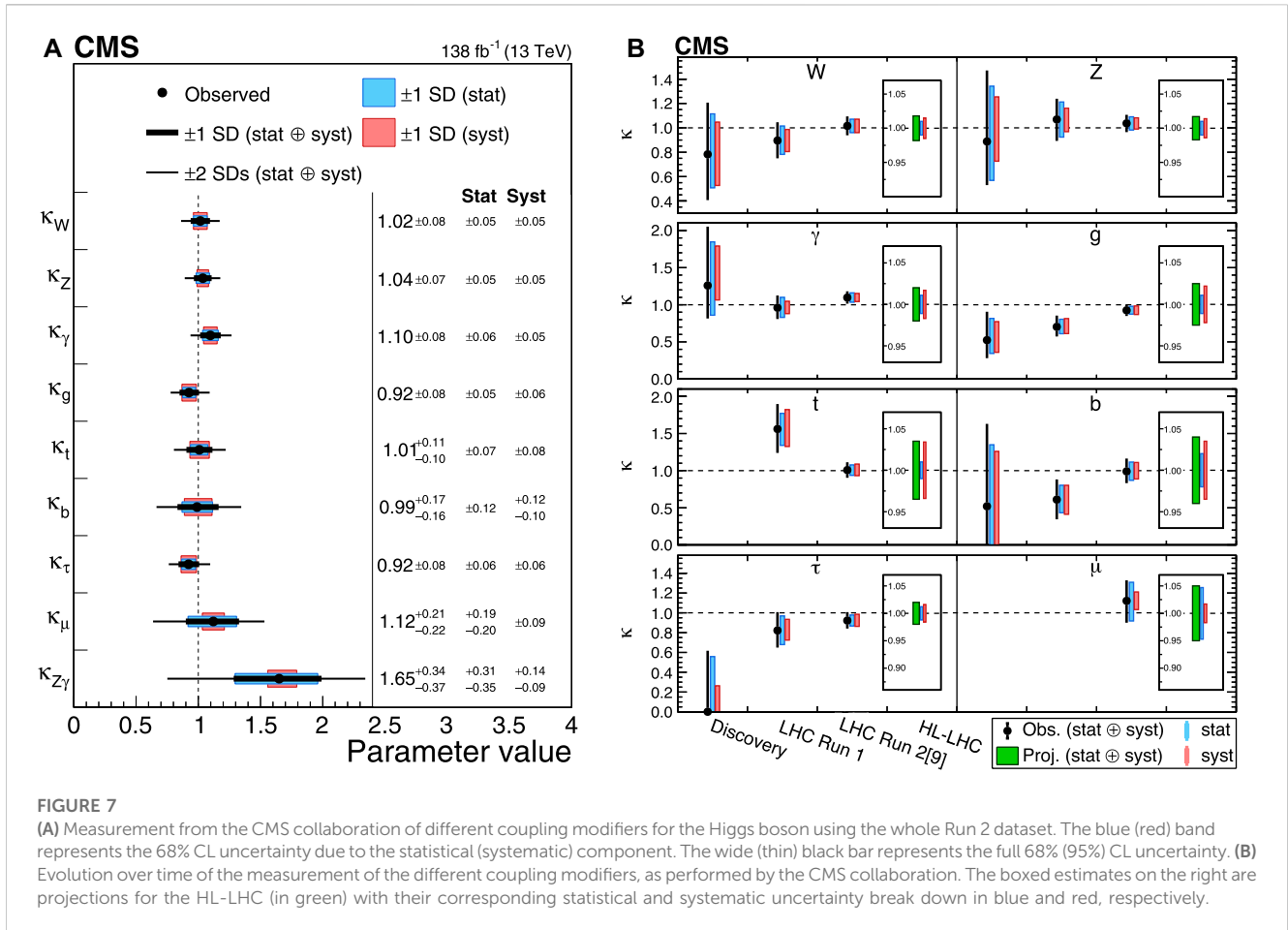
FIGURE 7
(A) Measurement from the CMS collaboration of different coupling modifiers for the Higgs boson using the whole Run 2 dataset. The blue (red) band represents the 68% CL uncertainty due to the statistical (systematic) component. The wide (thin) black bar represents the full 68% (95%) CL uncertainty. (B) Evolution over time of the measurement of the different coupling modifiers, as performed by the CMS collaboration. The boxed estimates on the right are projections for the HL-LHC (in green) with their corresponding statistical and systematic uncertainty break down in blue and red, respectively.

of Run 1, it was possible to measure κ_t and most couplings were known with an accuracy close to 10%. Moreover, in some cases such as κ_t, κ_b, and κ_g, the statistical uncertainty was already subdominant with respect to the systematic uncertainty. By the end of Run 2, which is our current knowledge, we passed the 10% threshold for most couplings. Systematic and statistical uncertainties are roughly the same size. Further reducing these uncertainties significantly will be very challenging at the LHC, and future machines will be better suited for this task, as discussed in Section 5. It is also possible to look for more specific BSM effects by imposing symmetries on the fit. For example, assuming that there is a universal coupling modifier for all couplings to vector bosons and a different one for all the couplings to fermions so that $\kappa_V = \kappa_Z = \kappa_W$ and $\kappa_f = \kappa_t = \kappa_\tau = \kappa_b = \kappa_\mu$. The effective couplings corresponding to loops in the gluon fusion and $H \to \gamma \gamma$ vertices are resolved in terms of their fundamental SM couplings. Figure 8 from the ATLAS collaboration (a similar result can be seen from the CMS collaboration in [9]) shows the two-dimensional fit on the κ_V and κ_f parameters, along with the contribution of each decay channel to it.

Since a combination, even within a single experiment, is an extremely challenging task, only a pair of cross-experiment Higgs physics combinations between ATLAS and CMS have been performed so far, both of them based on Run 1 data. They were aimed at measuring as precisely as possible the Higgs boson mass [55] and its couplings [56]. Further efforts on Run 2 are being

discussed between the collaborations, also targeting some rarer channels such as double-Higgs boson and $Z \gamma$ productions. The STXS scheme was developed to implement a compatible binning between the experiment and ease future combinations.

For a given value of the Higgs boson mass, the relationship between the mass of a SM particle and its coupling to the Higgs boson is well known in the SM. For bosons, it is represented as $\sqrt{\kappa} \frac{m}{vev}$, while for fermions, it is $\kappa \frac{m}{vev}$, where κ is the coupling modifier for that particular coupling and vev is the vacuum expectation value (~246 GeV). It is possible to check whether this relationship holds at the LHC with the measurements described so far. The results are similar for the CMS [9] and ATLAS [54] experiments. The measurements from the ATLAS collaboration are shown in Figure 9 and show a truly impressive agreement with the SM across four orders of magnitude in the couplings strength and three orders of magnitude in masses of the particles, one of the most stringent test of the SM in the Higgs sector that it is possible to develop.

4 The Higgs self-coupling

The potential of the Higgs field φ is given by $V(\varphi) = \frac{1}{2}m_H^2 \varphi^2 + \sqrt{\lambda/2}m_H \varphi^3 + \frac{1}{4}\lambda \varphi^4$, where the cubic term of strength λ represents the Higgs boson self-interaction. In the SM,
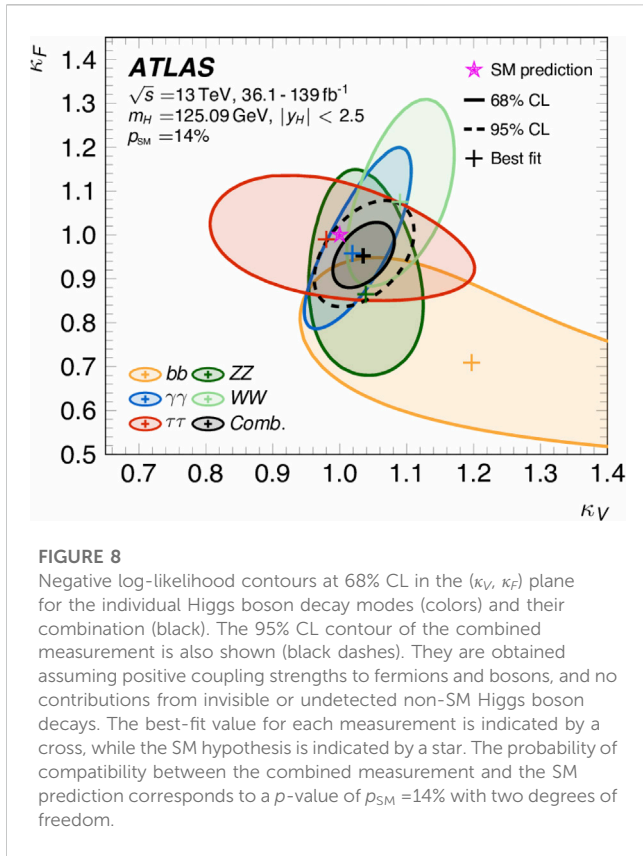
FIGURE 8
Negative log-likelihood contours at 68% CL in the (κ_V, κ_F) plane for the individual Higgs boson decay modes (colors) and their combination (black). The 95% CL contour of the combined measurement is also shown (black dashes). They are obtained assuming positive coupling strengths to fermions and bosons, and no contributions from invisible or undetected non-SM Higgs boson decays. The best-fit value for each measurement is indicated by a cross, while the SM hypothesis is indicated by a star. The probability of compatibility between the combined measurement and the SM prediction corresponds to a p-value of p_{SM} =14% with two degrees of freedom.
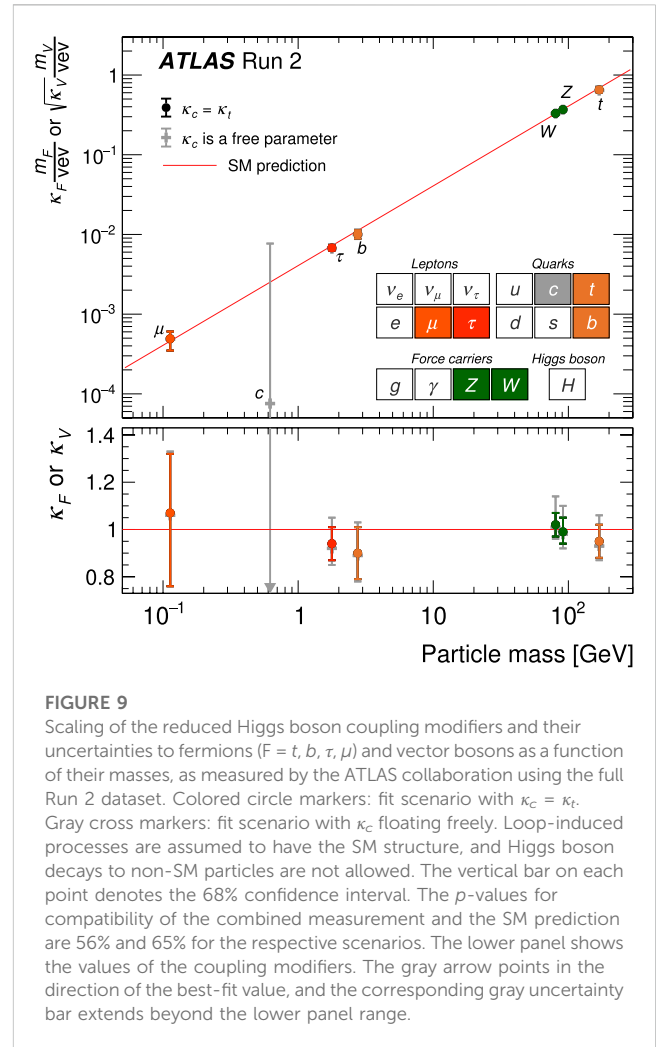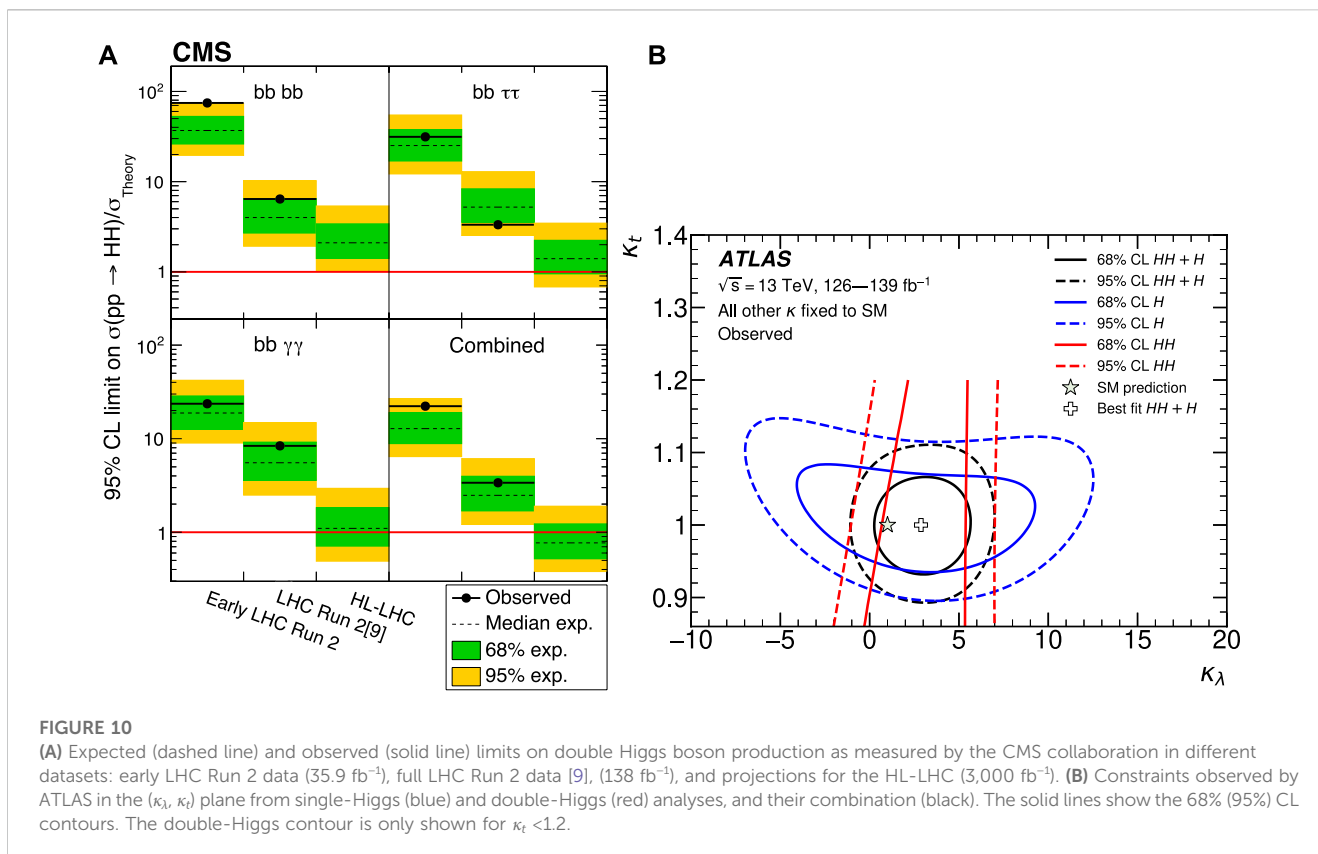

FIGURE 9
Scaling of the reduced Higgs boson coupling modifiers and their uncertainties to fermions (F = t, b, τ, μ) and vector bosons as a function of their masses, as measured by the ATLAS collaboration using the full Run 2 dataset. Colored circle markers: fit scenario with $\kappa_c = \kappa_t$. Gray cross markers: fit scenario with κ_c floating freely. Loop-induced processes are assumed to have the SM structure, and Higgs boson decays to non-SM particles are not allowed. The vertical bar on each point denotes the 68% confidence interval. The p-values for compatibility of the combined measurement and the SM prediction are 56% and 65% for the respective scenarios. The lower panel shows the values of the coupling modifiers. The gray arrow points in the direction of the best-fit value, and the corresponding gray uncertainty bar extends beyond the lower panel range.

$\lambda = m_{\mathrm{H}}^2 / (2vev^2)$. The shape of the potential is, therefore, determined by the value of the Higgs boson self-coupling, also known as the Higgs boson trilinear coupling and could be related to models of the strong first-order phase transition necessary for baryogenesis [57]. Since the Higgs boson acquires its mass through the self-interaction and since a Higgs boson loop is present in the Higgs boson propagator, the value of λ can be measured indirectly from the measurements of the Higgs boson couplings described in Section 3. Indeed, both CMS and ATLAS reported measurements obtained in this method, with CMS constraining the trilinear coupling in the region $-3.54 < \kappa_\lambda = \frac{\lambda}{\lambda^{\mathrm{SM}}} < 12.62$[9] and ATLAS at $-4.0 < \kappa_\lambda < 10.3$ [58].

At the LHC, it is possible to obtain a more direct measurement of this coupling by studying events where a pair of Higgs boson is produced. The study of double-Higgs events, where a pair of Higgs bosons is produced, was first suggested in the late 80s [59]. At the LHC, the most common production mode for Higgs boson pairs is via gluon fusion to H H. This can happen either through the production of an off-shell Higgs boson that subsequently decays into a pair of Higgs boson at their nominal mass or through the emission of a pair of Higgs bosons via a quark loop, as shown in the Feynman diagrams in Figures 2K, L. The two diagrams of Figures 2K, L produce a destructive interference among them, so the production cross section of double-Higgs events at the LHC is very small. For a center of mass energy of $\sqrt{s}$ = 13 TeV, it is just 32.76 fb [60–62] or less than 1/1000th of the single Higgs boson production cross section for the same energy (48 pb). Despite these events being exceedingly rare, the measurement of double-Higgs production has become one of the most interesting topics in the study of Higgs

physics at the LHC, and the experimental collaborations are obtaining more precise results with the ultimate goal of obtaining evidence of this process in the coming years. This effort is clear in Figure 10A, showing the limit obtained on the existence of double-Higgs event production for the three main channels studied by the CMS collaboration. The first results on H H production were obtained on data collected in 2016 [63]. By the end of Run 2, the limits have improved by a factor between 10 (b b b b) and 3 (b b γ γ), while over the same period, the luminosity grew only by a factor 4.

In order to obtain a significant number of events, the collaborations resort to explore as many final states as possible. The most sensitive channels, and the first ones to have been explored, are those where one of the Higgs bosons decays into a b $\bar{b}$ pair, i.e., $HH \rightarrow b$ $\bar{b}$ b $\bar{b}$, $HH \rightarrow b$ $\bar{b}$ γ γ, and $HH \rightarrow b$ $\bar{b}\tau\tau$. Since $H \rightarrow b$ $\bar{b}$ is the most common Higgs boson decay in the SM, these channels have a relatively high branching ratio among the double-Higgs boson decay at 33.92, 0.26, and 7.3%, respectively. Other less sensitive channels have also been explored with the latest results from ATLAS and CMS covering the b b b b, b b γ γ, b b τ τ, b b W W, and W W W W channels [58, 64–68]. Moreover, the CMS collaboration also reported measurements in the b b Z Z [69], W W τ τ and τ τ τ τ channels [70] and the ATLAS collaboration in the W W γ γ channel [68].

FIGURE 10
(A) Expected (dashed line) and observed (solid line) limits on double Higgs boson production as measured by the CMS collaboration in different datasets: early LHC Run 2 data (35.9 fb^{-1}), full LHC Run 2 data [9], (138 fb^{-1}), and projections for the HL-LHC (3,000 fb^{-1}). **(B)** Constraints observed by ATLAS in the (κ_λ, κ_t) plane from single-Higgs (blue) and double-Higgs (red) analyses, and their combination (black). The solid lines show the 68% (95%) CL contours. The double-Higgs contour is only shown for $\kappa_t <1.2$.

The combined results from the collaborations were able to put a constraint on the Higgs boson trilinear coupling at $-0.6 < \kappa_\lambda < 6.6$ (ATLAS) and $-1.2 < \kappa_\lambda < 6.5$ (CMS) using the double-Higgs events alone. It must be noted that since it is not possible to distinguish between events coming from the Higgs boson trilinear interaction (Figure 2K) or from the quark loop (Figure 2L), these measurements rely on the assumption that $\kappa_t = 1$ and that all possible deviations are only due to effects from κ_λ. To overcome this limitation and to increase the sensitivity on κ_λ, the collaborations and the theory community are working on the combination of double- and single-Higgs measurements, where it would be possible to constrain separately the two couplings. Such an effort was recently shown by the ATLAS collaboration [57]. The final result is still dominated by the double-Higgs boson production sensitivity, with a final constraint of $-0.4 < \kappa_\lambda < 6.3$. The importance of the single Higgs measurement contribution in breaking the degeneracy between κ_λ and κ_t can be observed in Figure 10B, showing the constraints obtained in the $\kappa_\lambda - \kappa_t$ plane by single- and double-Higgs measurements and their combination.

5 Where we are heading to

The LHC plans to continue to collect data at $\sqrt{s} = 13.6$ TeV until 2025, when the end of Run 3 will conclude the LHC physics program. Run 3 is expected to deliver at least 250 fb^{-1}. In addition to improving on the precision of the couplings discussed so far, the additional data gathered in the next few years will provide enough integrated luminosity to reach a precision on most couplings close to 5%–10% (40% for κ_μ), and should start gathering evidence for the presence of the Higgs boson trilinear coupling with $\kappa_\lambda > 0$.

After 2025, the LHC will undergo a major overhaul, with the goal of reopening in 2029 with a new machine capable of running at an instantaneous luminosity 3–4 times higher than the LHC. The resulting machine has been named high-luminosity LHC (HL-LHC), and it is planned to deliver between 3,000 and 4,000 fb^{-1} at a center of mass energy of 14 TeV by 2041. Both the ATLAS and CMS experiments will need substantial upgrades in order to be able to collect data at the HL-LHC, with the major challenge being posed by the pile-up, which will rise up to an average of 200 pile-up collisions for each hard proton–proton scattering. Timing detectors, ultrafast triggers, and much more granular trackers will be among the strategies deployed in order to maintain, if not improve, the current experiment performances. This amount of luminosity will allow constraining the Higgs boson coupling to most SM particles at around 2%–4%, including the Higgs boson coupling to muons, as shown in Figure 11A. To appreciate the improvement with respect to the LHC measurement, it is possible to compare the current LHC measurements with the projected HL-LHC performances in Figure 7B, where the small inset on the right shows the HL-LHC projections. At these sensitivities, even relatively small deviations from the SM should start to be visible [71]. Among the most important targets for the Higgs boson couplings at the HL-LHC, there will be precise measurements of the Higgs boson decay into
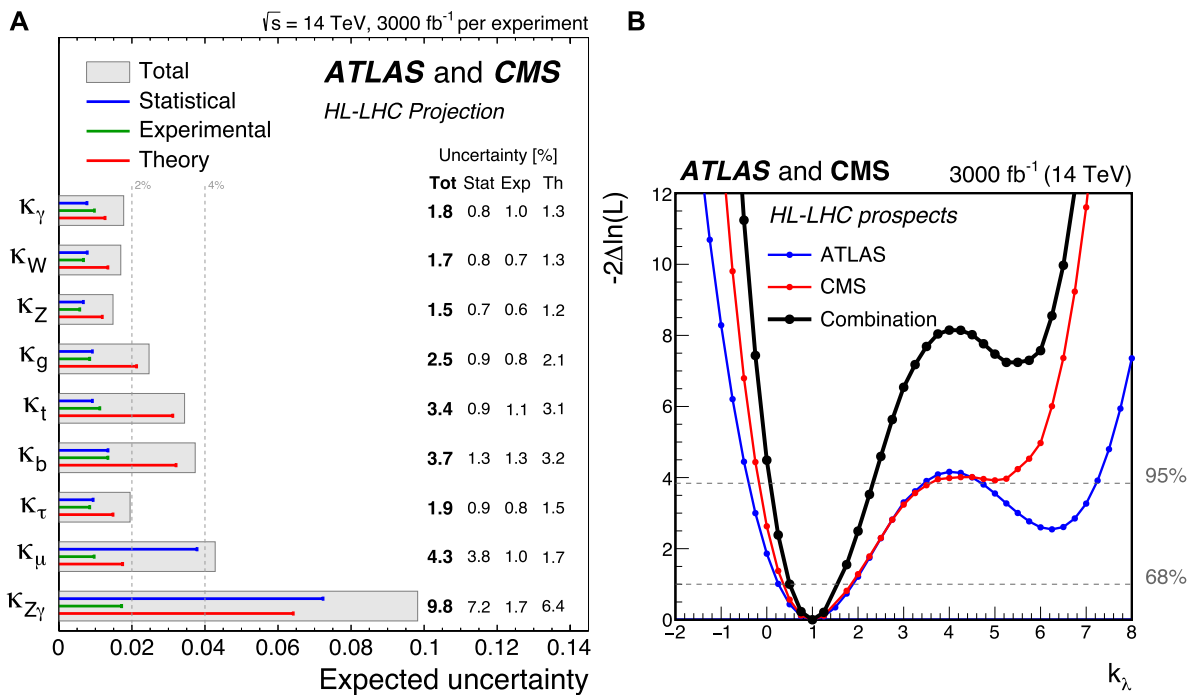
FIGURE 11
(A) Summary plot showing the total expected ±1σ uncertainties on the coupling modifier parameters for the combination of ATLAS and CMS extrapolations to the HL-LHC. For each measurement, the total uncertainty is indicated by a gray box, while the statistical, experimental, and theory uncertainties are indicated by a blue, green, and red line, respectively. The projections assume reduced experimental systematic uncertainties, according to the expectations for HL-LHC. **(B)** Expected likelihood scan as a function of $\kappa_\lambda = \lambda_{HHH}/\lambda_{SM}$ for HL-LHC. The blue (red) line corresponds to the combined ATLAS (CMS) projection, with the black line being the combination of the two experiments.

muons. On the double-Higgs side, it will be possible to obtain evidence of the existence of double-Higgs boson production, with an expected significance of approximately 4.0 and a projected precision on the double-Higgs boson production of roughly 50% [71]. It could be possible to measure the first hints of *ttHH* production [72]. Figure 10A shows the expected evolution for the limit on the double-Higgs boson production cross section, with the combined limit going below the threshold of 1, meaning that the sensitivity is sufficient to establish the existence of the Higgs boson pair production. It is expected that in the absence of new physics and by combining results from both CMS and ATLAS, the constraints on the Higgs boson trilinear coupling will be set in the region $0.52 < \kappa_\lambda < 1.5$ [71], as shown in Figure 11B.

In order to reach even tighter constraints on the couplings and to observe the Higgs boson coupling to light particles such as the *c*-quark, completely new machines will be needed, which are currently in their exploratory phases. A couple of the most promising proposals that are being circulated will be briefly discussed here.

The Future Circular Collider (FCC) is a collider with a circumference of 90–100 km capable of running both as a lepton–lepton (FCC-ee) [73], lepton–hadron (FCC-eh), and hadron–hadron (FCC-hh) [74] collider, which should be built in the area of CERN. The FCC-hh will deliver 30 ab^{-1} of proton–proton collisions at the center-of-mass energy of $\sqrt{s}$ = 100 TeV over an operating time of 25 years. Such a powerful machine will greatly

enhance the precision achievable in the Higgs sector. When considering the improvement in the knowledge of the SM cross sections and the results obtained during the FCC-ee and FCC-eh data collection, FCC-hh is projected to measure the Higgs boson couplings well below the percent precision [75]. It is particularly impressive to see a projected sensitivity at the percentage level on the Higgs boson coupling to the *c*-quark (κ_c). Figure 12 shows the projected FCC performances compared to some other proposed future colliders and the HL-LHC. One of the main targets of the FCC-hh program is the precise determination of the Higgs boson trilinear coupling. The employed techniques are similar to those established at the LHC with the same main channels considered, although the much larger available dataset will allow obtaining a greater precision on this measurement. Projections have shown that by combining all main channels together and depending on assumption on the detector performances and systematic uncertainties, FCC-hh could measure the Higgs boson trilinear coupling with a precision between 3.4% and 7.8% [76], as shown in Figure 13.

FCC will be a monumental task to complete, and it is difficult to imagine even larger colliders to be built in the future. To reach energies higher than what FCC would be capable of, new technologies must be deployed. One such proposal is the Muon Collider. Collisions between leptons provide a much cleaner environment with respect to proton–proton collision, but it is difficult to reach high energies colliding particles as light as electrons. One solution is to operate a
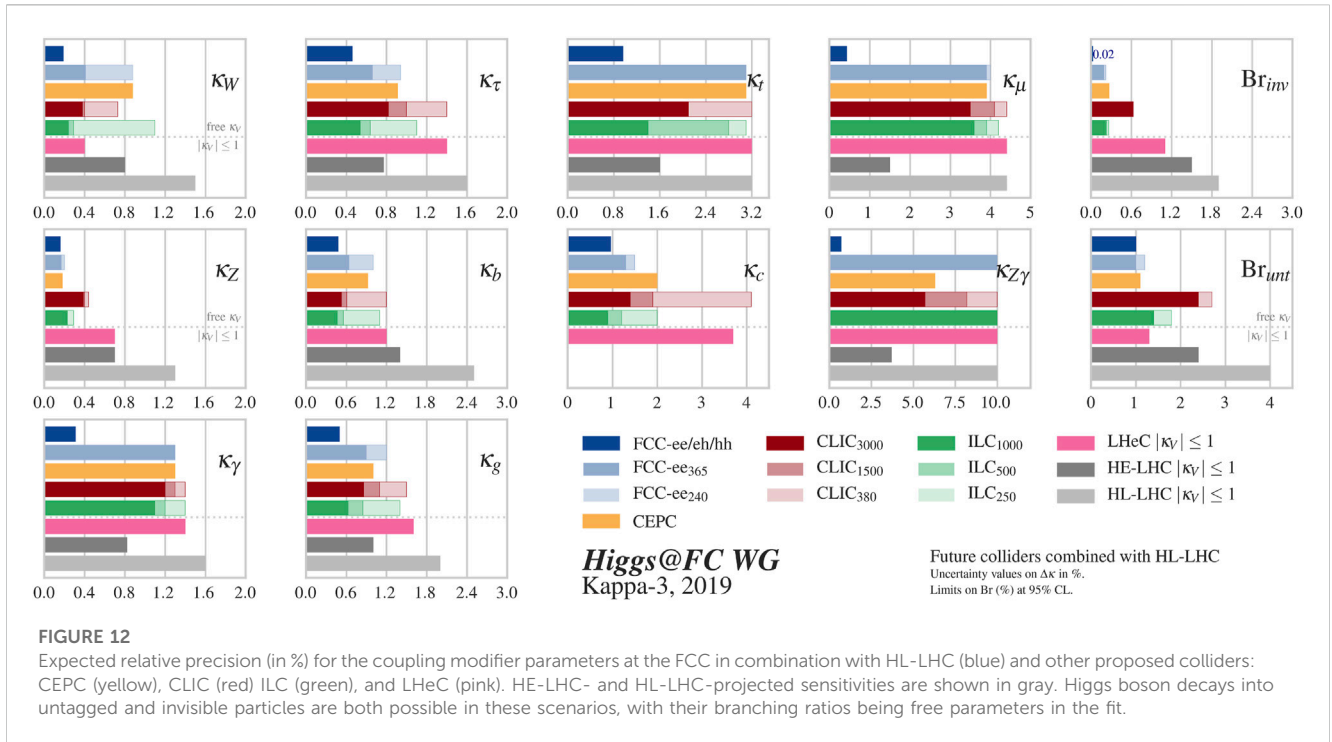
FIGURE 12
Expected relative precision (in %) for the coupling modifier parameters at the FCC in combination with HL-LHC (blue) and other proposed colliders: CEPC (yellow), CLIC (red) ILC (green), and LHeC (pink). HE-LHC- and HL-LHC-projected sensitivities are shown in gray. Higgs boson decays into untagged and invisible particles are both possible in these scenarios, with their branching ratios being free parameters in the fit.
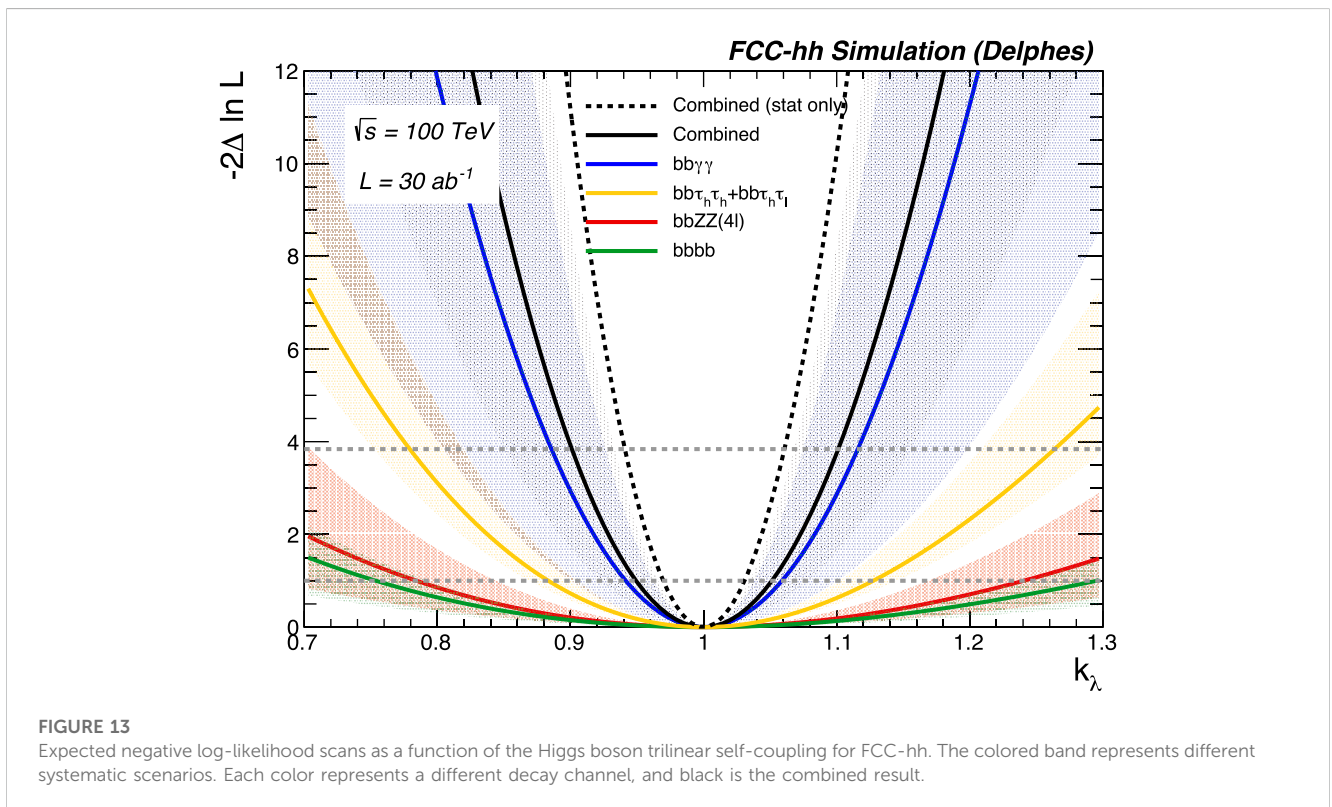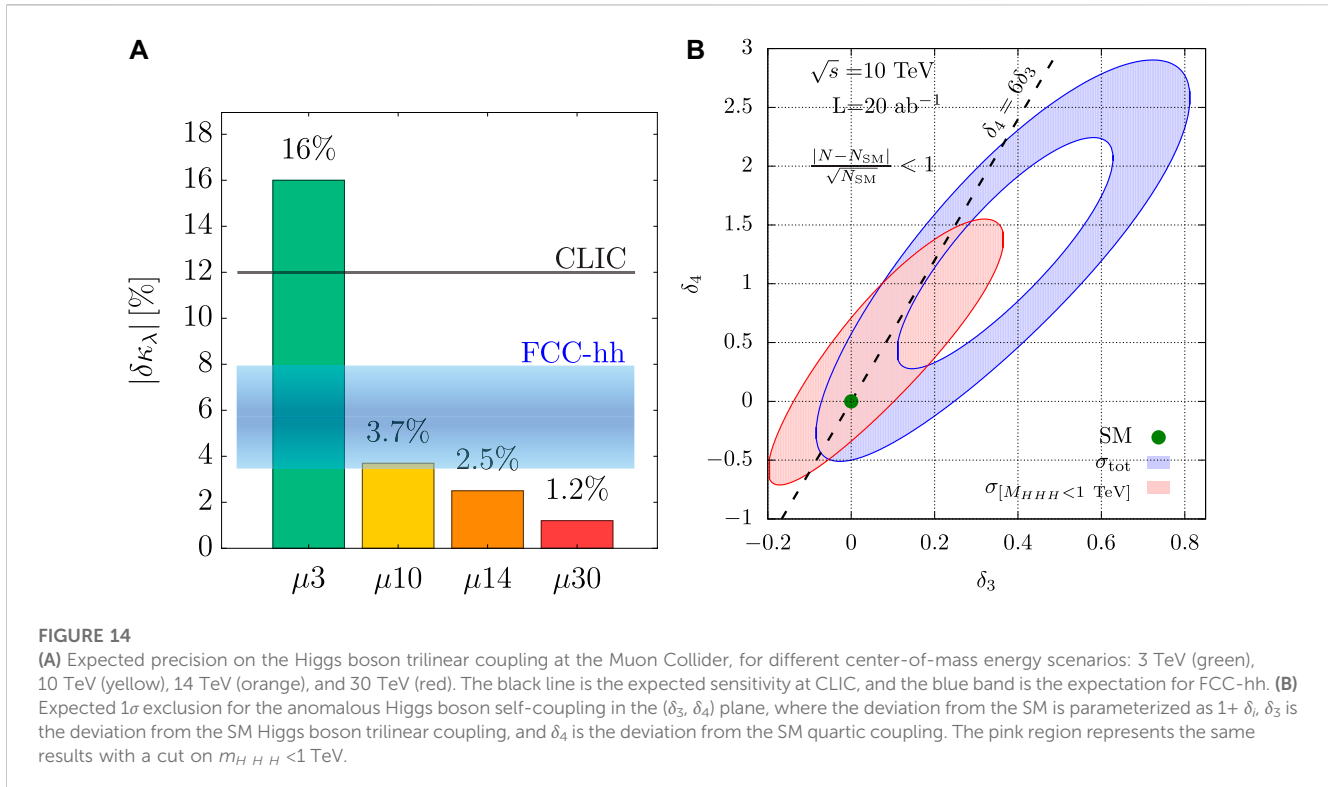

FIGURE 13
Expected negative log-likelihood scans as a function of the Higgs boson trilinear self-coupling for FCC-hh. The colored band represents different systematic scenarios. Each color represents a different decay channel, and black is the combined result.

lepton collider, but colliding muons instead of electrons and thus exploiting the much larger mass of the muon to reach higher center-of-mass energies. The idea is not new. The possibility of building muon storage rings was first mentioned in the 60s [77], and the idea of

using heavy leptons, such as muons instead of electrons, has been floating around since the 70s, although building one such machine was technically impractical until now. The main technical issues for a Muon Collider, which we are now managing to address, are that the

FIGURE 14
(A) Expected precision on the Higgs boson trilinear coupling at the Muon Collider, for different center-of-mass energy scenarios: 3 TeV (green), 10 TeV (yellow), 14 TeV (orange), and 30 TeV (red). The black line is the expected sensitivity at CLIC, and the blue band is the expectation for FCC-hh. **(B)** Expected 1σ exclusion for the anomalous Higgs boson self-coupling in the (δ_3, δ_4) plane, where the deviation from the SM is parameterized as $1+\delta_i$, δ_3 is the deviation from the SM Higgs boson trilinear coupling, and δ_4 is the deviation from the SM quartic coupling. The pink region represents the same results with a cut on m_{HHH} <1 TeV.

muons must be accelerated very quickly in order to boost their lifetime in the laboratory frame before they decay since their proper lifetime is only 2.2 μs. Moreover, the decay of muons inside the beam will generate a large beam-induced background that must be controlled. Nevertheless, the first estimation for the physics reach of the Muon Collider is very promising. The current proposal suggests operating a Muon Collider at $\sqrt{s}$ = 3 TeV and $\sqrt{s}$ = 10 TeV, although other configurations are also under study. It must be noted that although these energies are nominally one order of magnitude lower than what will be available at FCC-hh, in the case of the Muon Collider, the whole center of mass energy is available in the hard scattering, while in hadron collisions, only the fraction of energy carried by the two heavily interacting partons participates in the hard scattering. The energy of FCC-hh roughly corresponds to a 14-TeV Muon Collider [78], which would require a collider of 14 km of circumference, instead of the 100 km of FCC. The first projections show that depending on the actual configuration, the Muon Collider can reach sensitivities close to those obtained at FCC-hh, with a precision of O (0.1%) on the coupling to vector boson and of 1% on κ_c [79]. Where the muon collider show a potential to outperform even the FCC is in the Higgs boson trilinear and quartic couplings, measured in events with two and three Higgs bosons in the final state, respectively. As shown in Figure 14A the Muon Collider, when operating at 10 TeV, can potentially reach a 3.7% uncertainty on κ_λ, at the lower edge of the FCC band, and can reach even higher sensitivities if larger machines are built. Studies have also been performed on the capabilities of Muon Collider machines to measure triple-Higgs boson production [80], showing that a 10 TeV machine could measure the quartic-Higgs boson self-coupling with roughly 50% accuracy, as shown in Figure 14B.

6 Conclusion

The discovery of the Higgs boson at the CERN LHC by the ATLAS and CMS collaborations unleashed a new era of measurements of the Higgs sector. Among the studies of the properties of the Higgs boson are its couplings with the particles of the SM, which are a direct test of the electroweak symmetry breaking.

In the 10 years since the discovery, the LHC made huge improvements in luminosity delivered and in energy available in the center of mass. The experiments on their side adapted to these evolving conditions by developing ever more refined analysis tools and strategies. This allowed progressing from testing the more common production modes such as ggH and VBF, and the decay modes with the best signal-over-background ratio such as $H \rightarrow \gamma\gamma$, $H \rightarrow ZZ$, and $H \rightarrow WW$ to ever more comprehensive measurements. The latest combined fits address all the main production and decay mechanisms of the Higgs boson, including the first exploration of the Higgs boson self-coupling. The results obtained by the experiments running at the LHC show a remarkable agreement with the SM prediction, spanning three orders in magnitude in mass and four in the coupling values, with no significant deviations observed so far.

Nevertheless, there still is plenty of phase space available for possible deviations from the SM, in what could be an indication of higher-energy BSM effects. To tackle these effects and to narrow the uncertainties on the couplings, the HL-LHC upgrade planned for 2029 will deliver 10 times the luminosity of the LHC. This will allow reducing the uncertainty on the couplings down to the 2% level and will make channels such as $\mu\mu$ and $Z\gamma$ accessible for precision

studies, as well as providing a definite observation of *HH* production.

Even at the HL-LHC, coupling to first- and second-generation fermions will remain elusive. Constraints below the 1% level and measurement of processes such as $H \rightarrow c\,c$ can be obtained at future facilities, such as the FCC and the Muon Collider, which are also projected to obtain a few percentage-level precision on the *H H* production.

Author contributions

All authors listed have made a substantial, direct, and intellectual contribution to the work and approved it for publication.

Conflict of interest

The authors declare that the research was conducted in the absence of any commercial or financial relationships that could be construed as a potential conflict of interest.

Publisher's note

All claims expressed in this article are solely those of the authors and do not necessarily represent those of their affiliated organizations, or those of the publisher, the editors, and the reviewers. Any product that may be evaluated in this article, or claim that may be made by its manufacturer, is not guaranteed or endorsed by the publisher.

References

1. Aad G, Abat E, Abdallah J, Abdelalim AA, Abdesselam A, et al. The ATLAS experiment at the CERN large hadron collider. *JINST* (2008) 3:S08003. doi:10.1088/1748-0221/3/08/S08003

2. Chatrchyan S, Hmayakyan G, Khachatryan V, Sirunyan AM, Adam W, et al. The CMS experiment at the CERN LHC. *JINST* (2008) 3:S08004. doi:10.1088/1748-0221/3/08/S08004

3. Aad G, Abajyan T, Abbott B, Abdallah J, Abdel Khalek S, Abdelalim AA, et al. Improved luminosity determination in pp collisions at $\sqrt{s} = 7\,\mathrm{TeV}$ using the ATLAS detector at the LHC. *Eur Phys J C* (2013) 73:2518. doi:10.1140/epjc/s10052-013-2518-3

4. ATLAS Collaboration. *Luminosity determination in pp collisions at $\sqrt{s} =13$ √s=13 TeV using the ATLAS detector at the LHC* (2022). *arXiv [preprint]*.

5. ATLAS Collaboration. *Preliminary analysis of the luminosity calibration of the ATLAS 13.6 TeV data recorded in 2022* (2023). *CERN Document Server [preprint]*.

6. CMS Collaboration. *CMS luminosity based on pixel cluster counting—summer 2013 update* (2013). *CERN Document Server [preprint]*.

7. Sirunyan AM, Tumasyan A, Adam W, Andrejkovic JW, Bergauer T, Chatterjee S, et al. Precision luminosity measurement in proton–proton collisions at $\sqrt{s} = 13\,\hbox{TeV}$ in 2015 and 2016 at CMS. *Eur Phys J C* (2021) 81:800. doi:10.1140/epjc/s10052-021-09538-2

8. CMS Collaboration. *Luminosity monitoring with Z counting in early 2022 data* (2023). *CERN Document Server [preprint]*.

9. CMS Collaboration. A portrait of the Higgs boson by the CMS experiment ten years after the discovery. *Nature* (2022) 607:60–8. doi:10.1038/s41586-022-04892-x

10. de Florian D. Handbook of LHC Higgs cross sections: 4. Deciphering the nature of the Higgs sector. *CERN Yellow Rep Monogr* (2016) 2017. doi:10.23731/CYRM-2017-002

11. David A, Denner A, Duehrssen M, Grazzini M, Grojean C, Passarino G, et al. *LHC HXSWG interim recommendations to explore the coupling structure of a Higgs-like particle* (2012). *arXiv [preprint]*.

12. Andersen JR, Artoisenet P, Bagnaschi EA, Banfi A, Becher T, Bernlochner FU, et al. Handbook of LHC Higgs cross sections: 3. Higgs properties. *CERN Yellow Rep Monogr* (2013) 2013. doi:10.5170/CERN-2013-004

13. Monti F, Pandini CE, Lucio Alves FL, Yang H, Huang Y, Wang J, et al. *Modelling of the single-Higgs simplified template cross-sections (STXS 1.2) for the determination of the Higgs boson trilinear self-coupling* (2022). *CERN Document Server [preprint]*.

14. Englert F, Brout R. Broken symmetry and the mass of gauge vector mesons. *Phys Rev Lett* (1964) 13:321–3. doi:10.1103/PhysRevLett.13.321

15. Higgs PW. Broken symmetries, massless particles and gauge fields. *Phys Lett* (1964) 12:132–3. doi:10.1016/0031-9163(64)91136-9

16. Higgs PW. Broken symmetries and the masses of gauge bosons. *Phys Rev Lett* (1964) 13:508–9. doi:10.1103/PhysRevLett.13.508

17. Guralnik GS, Hagen CR, Kibble TWB. Global conservation laws and massless particles. *Phys Rev Lett* (1964) 13:585–7. doi:10.1103/PhysRevLett.13.585

18. Higgs PW. Spontaneous symmetry breakdown without massless bosons. *Phys Rev* (1966) 145:1156–63. doi:10.1103/PhysRev.145.1156

19. Kibble TWB. Symmetry breaking in nonAbelian gauge theories. *Phys Rev* (1967) 155:1554–61. doi:10.1103/PhysRev.155.1554

20. Chatrchyan S, Khachatryan V, Sirunyan A, Tumasyan A, Adam W, Aguilo E, et al. Observation of a new boson at a mass of 125 GeV with the CMS experiment at the LHC. *Phys Lett B* (2012) 716:30–61. doi:10.1016/j.physletb.2012.08.021

21. Aad G, Abajyan T, Abbott B, Abdallah J, Abdel Khalek S, Abdelalim A, et al. Observation of a new particle in the search for the Standard Model Higgs boson with the ATLAS detector at the LHC. *Phys Lett B* (2012) 716:1–29. doi:10.1016/j.physletb.2012.08.020

22. Sirunyan AM, Tumasyan A, Adam W, Andrejkovic JW, Bergauer T, Chatterjee S, et al. Measurements of Higgs boson production cross sections and couplings in the diphoton decay channel at $\sqrt{\mathrm{s}}$ = 13 TeV. *JHEP* (2021) 07:027. doi:10.1007/JHEP07(2021)027

23. ATLAS, Aad G, Abbott B, Abbott DC, Abeling K, Abidi SH, et al. Measurement of the properties of Higgs boson production at √s=13 TeV in the $H \rightarrow \gamma\gamma$ channel using 139 fb⁻¹ of pp collision data with the ATLAS experiment. *JHEP. arXiv* (2023) 07:088. doi:10.1007/JHEP07(2023)088

24. Aad G, Abbott B, Abbott DC, Abud AA, Abeling K, Abhayasinghe DK, et al. Higgs boson production cross-section measurements and their EFT interpretation in the 4ℓ decay channel at √s=13 TeV with the ATLAS detector. *Eur Phys J C* (2020) 80 957. doi:10.1140/epjc/s10052-020-8227-9

25. De Rujula A, Lykken J, Pierini M, Rogan C, Spiropulu M. Higgs boson look-alikes at the LHC. *Phys Rev D* (2010) 82:013003. doi:10.1103/PhysRevD.82.013003

26. Chatrchyan S, Khachatryan V, Sirunyan AM, Tumasyan A, Adam W, Bergauer T, et al. Search for a Higgs boson in the decay channel H to ZZ(*) to q qbar ℓ^- l+ in pp collisions at √s=7 TeV. *JHEP* (2012) 04:036. doi:10.1007/JHEP04(2012)036

27. Chatrchyan S, Khachatryan V, Sirunyan A, Tumasyan A, Adam W, Bergauer T, et al. Measurement of the properties of a Higgs boson in the four-lepton final state. *Phys Rev D* (2014) 89:092007. doi:10.1103/PhysRevD.89.092007

28. Aad G, Abbott B, Abdallah J, Abdel Khalek S, Abdinov O, Aben R, et al. Measurements of Higgs boson production and couplings in the four-lepton channel in pp collisions at center-of-mass energies of 7 and 8 TeV with the ATLAS detector. *Phys Rev D* (2015) 91:012006. doi:10.1103/PhysRevD.91.012006

29. Sirunyan AM, Tumasyan A, Adam W, Andrejkovic JW, Bergauer T, et al. Measurements of production cross sections of the Higgs boson in the four-lepton final state in proton–proton collisions at $\sqrt{s} = 13\,\text{TeV}$. *Eur Phys J C* (2021) 81:488. doi:10.1140/epjc/s10052-021-09200-x

30. ATLAS. *Measurements of Higgs boson production by gluon–gluon fusion and vector-boson fusion using H → WW* → eνμν decays in pp collisions at √s=13 TeV with the ATLAS detector* (2022). *arXiv*.

31. CMS, Tumasyan A, Adam W, Andrejkovic JW, Bergauer T, Chatterjee S, et al. Measurements of the Higgs boson production cross section and couplings in the W boson pair decay channel in proton-proton collisions at √s=13 TeV. *Eur Phys J C* (2023) 83 (7):667. *arXiv*. doi:10.1140/epjc/s10052-023-11632-6

32. Sirunyan AM, Tumasyan A, Adam W, Ambrogi F, Asilar E, Bergauer T, et al. Observation of the Higgs boson decay to a pair of τ leptons with the CMS detector. *Phys Lett B* (2018) 779:283–316. doi:10.1016/j.physletb.2018.02.004

33. Aaboud M, Aad G, Abbott B, Abdinov O, Abeloos B, Abhayasinghe D, et al. Cross-section measurements of the Higgs boson decaying into a pair of τ-leptons in proton-proton collisions at √s=13 TeV with the ATLAS detector. *Phys Rev D* (2019) 99:072001. doi:10.1103/PhysRevD.99.072001

34. Elagin A, Murat P, Pranko A, Safonov A. A new mass reconstruction technique for resonances decaying to. *Nucl Instrum Meth A* (2011) 654:481–9. doi:10.1016/j.nima.2011.07.009

35. Bianchini L, Conway J, Friis EK, Veelken C. Reconstruction of the Higgs mass in $H \rightarrow \tau\tau$ events by dynamical likelihood techniques. *J Phys Conf Ser* (2014) 513:022035. doi:10.1088/1742-6596/513/2/022035

36. Sirunyan AM, Tumasyan A, Adam W, Bergauer T, Dragicevic M, Erö J, et al. Evidence for Higgs boson decay to a pair of muons. *JHEP* (2021) 01:148. doi:10.1007/JHEP01(2021)148

37. Qu H, Gouskos L. ParticleNet: Jet tagging via particle clouds. *Phys Rev D* (2020) 101:056019. doi:10.1103/PhysRevD.101.056019

38. Bols E, Kieseler J, Verzetti M, Stoye M, Stakia A. Jet flavour classification using DeepJet. *JINST* (2020) 15:P12012. doi:10.1088/1748-0221/15/12/P12012

39. Tumasyan A, Adam W, Andrejkovic JW, Bergauer T, Chatterjee S, Dragicevic M, et al. A new calibration method for charm jet identification validated with proton-proton collision events at $\sqrt{s}$ = 13 TeV. *JINST* (2022) 17:P03014. doi:10.1088/1748-0221/17/03/P03014

40. ATLAS, Aad G, Abbott B, Abbott DC, Abeling K, Abidi SH, et al. (2023). *arXiv* 83 (7):681. doi:10.1140/epjc/s10052-023-11699-1

41. CMS Collaboration. *Performance of the ParticleNet tagger on small and large-radius jets at high level trigger in run 3* (2023). *CERN Document Server* [preprint].

42. Aaboud M, Aad G, Abbott B, Abdinov O, Abeloos B, Abhayasinghe D, et al. Observation of H→bb̄ decays and *VH* production with the ATLAS detector. *Phys Lett B* (2018) 786:59–86. doi:10.1016/j.physletb.2018.09.013

43. Aad G, Abbott B, Abbott DC, Abud AA, Abeling K, et al. Measurements of Higgs bosons decaying to bottom quarks from vector boson fusion production with the ATLAS experiment at $\sqrt{s}=13\,\text{TeV}$. *Eur Phys J C* (2021) 81:537. doi:10.1140/epjc/s10052-021-09192-8

44. Sirunyan AM, Tumasyan A, Adam W, Ambrogi F, Bergauer T, Dragicevic M, et al. Inclusive search for highly boosted Higgs bosons decaying to bottom quark-antiquark pairs in proton-proton collisions at $\sqrt{s}$ = 13 TeV. *JHEP* (2020) 12:085. doi:10.1007/JHEP12(2020)085

45. CMS, Tumasyan A, Adam W, Andrejkovic JW, Bergauer T, Chatterjee S, et al. Search for Higgs boson decay to a charm quark-antiquark pair in proton-proton collisions at $\sqrt{s}$=13 TeV. *Phys Rev Lett* (2023). *arXiv* 131 (6):061801. doi:10.1103/PhysRevLett.131.061801

46. Aad G, Abbott B, Abbott DC, Abud AA, Abeling K, Abhayasinghe DK, et al. Direct constraint on the Higgs-charm coupling from a search for Higgs boson decays into charm quarks with the ATLAS detector. *Eur Phys J C* (2022) 82:717. doi:10.1140/epjc/s10052-022-10588-3

47. CMS, Tumasyan A, Adam W, Andrejkovic JW, Bergauer T, Chatterjee S, et al. Search for boosted Higgs boson decay to a charm quark-antiquark $\sqrt{s}$=13 TeV. *Phys Rev Lett* (2023). *arXiv* 131 (4):041801. doi:10.1103/PhysRevLett.131.041801

48. The SLD Electroweak. *A Combination of preliminary electroweak measurements and constraints on the standard model* (2003). *arXiv* [preprint].

49. Aaboud M, Aad G, Abbott B, Abdinov O, Abeloos B, Abhayasinghe D, et al. Observation of Higgs boson production in association with a top quark pair at the LHC with the ATLAS detector. *Phys Lett B* (2018) 784:173–91. doi:10.1016/j.physletb.2018.07.035

50. Sirunyan AM, Tumasyan A, Adam W, Ambrogi F, Asilar E, Bergauer T, et al. Observation of ttH production. *Phys Rev Lett* (2018) 120:231801. doi:10.1103/PhysRevLett.120.231801

51. Sirunyan AM, Tumasyan A, Adam W, Bergauer T, Dragicevic M, et al.CMS Collaboration Measurement of the Higgs boson production rate in association with top quarks in final states with electrons, muons, and hadronically decaying tau leptons at $\sqrt{s}$=13 TeV. *Eur Phys J C* (2021) 81:378. doi:10.1140/epjc/s10052-021-09014-x

52. ATLAS, CMS; LHC Higgs Combination Group. *Procedure for the LHC Higgs boson search combination in Summer 2011* (2011). *CERN Document Server* [preprint].

53. Sirunyan AM, Tumasyan A, Adam W, Ambrogi F, Asilar E, Bergauer T, et al. Combined measurements of Higgs boson couplings in proton–proton collisions at $\sqrt{s}=13\,\text{Te}\text{V}$. *Eur Phys J C* (2019) 79:421. doi:10.1140/epjc/s10052-019-6909-y

54. ATLAS Collaboration. A detailed map of Higgs boson interactions by the ATLAS experiment ten years after the discovery. *Nature* (2022) 607:52–9. doi:10.1038/s41586-022-04893-w

55. Aad G, Abbott B, Abdallah J, Abdinov O, Aben R, Abolins M, et al. Combined measurement of the Higgs boson mass in *pp* collisions at $\sqrt{s}$=7 and 8 TeV with the ATLAS and CMS experiments. *Phys Rev Lett* (2015) 114:191803. doi:10.1103/PhysRevLett.114.191803

56. Aad G, Abbott B, Abdallah J, Abdinov O, Abeloos B, Aben R, et al. Measurements of the Higgs boson production and decay rates and constraints on its couplings from a combined ATLAS and CMS analysis of the LHC pp collision data at s = 7 $\sqrt{s}=7$ and 8 TeV. *JHEP* (2016) 08:045. doi:10.1007/JHEP08(2016)045

57. Barrow JD, Turner MS. Baryosynthesis and the origin of galaxies. *Nature* (1981) 291:469–72. doi:10.1038/291469a0

58. ATLAS CollaborationAbbott B, Abbott D, Abeling K, Abidi S, Aboulhorma A, et al. Constraints on the Higgs boson self-coupling from single- and double-Higgs production with the ATLAS detector using pp collisions at s=13 TeV. *Phys Lett B* (2023) 843:137745. doi:10.1016/j.physletb.2023.137745

59. Eboli OJP, Marques GC, Novaes SF, Natale AA. Twin Higgs boson production. *Phys Lett B* (1987) 197:269–72. doi:10.1016/0370-2693(87)90381-9

60. Grazzini M, Heinrich G, Jones S, Kallweit S, Kerner M, Lindert JM, et al. Higgs boson pair production at NNLO with top quark mass effects. *JHEP* (2018) 05:059. doi:10.1007/JHEP05(2018)059

61. Baglio J, Campanario F, Glaus S, Mühlleitner M, Ronca J. Spira mgg → HH: Combined uncertainties. *Phys Rev D* (2021) 103:056002. doi:10.1103/PhysRevD.103.056002

62. Dreyer FA, Karlberg A. Vector-boson fusion Higgs pair production at N³LO. *Phys Rev D* (2018) 98:114016. doi:10.1103/PhysRevD.98.114016

63. Sirunyan AM, Tumasyan A, Adam W, Ambrogi F, Asilar E, Bergauer T, et al. Combination of searches for Higgs boson pair production in proton-proton collisions at $\sqrt{s}$= 13 TeV. *Phys Rev Lett* (2019) 122:121803. doi:10.1103/PhysRevLett.122.121803

64. Tumasyan A, Adam W, Andrejkovic J, Bergauer T, Chatterjee S, Damanakis K, et al. Search for Higgs boson pair production in the four b quark final state in proton-proton collisions at s=13 TeV. *Phys Rev Lett* (2022) 129:081802. doi:10.1103/PhysRevLett.129.081802

65. CMS, Tumasyan A, Adam W, Andrejkovic JW, Bergauer T, Chatterjee S, et al. Search for nonresonant pair production of highly energetic Higgs bosons decaying to bottom quarks. *Phys Rev Lett* (2023). *arXiv* 131 (4):041803. doi:10.1103/PhysRevLett.131.041803

66. Tumasyan A, Adam W, Andrejkovic J, Bergauer T, Chatterjee S, Damanakis K, et al. Search for nonresonant Higgs boson pair production in final state with two bottom quarks and two tau leptons in proton-proton collisions at s=13 TeV. *Phys Lett B* (2023) 842:137531. doi:10.1016/j.physletb.2022.137531

65. Sirunyan AM, Tumasyan A, Adam W, Bergauer T, Dragicevic M, Escalante Del Valle A, et al. Search for nonresonant Higgs boson pair production in final states with two bottom quarks and two photons in proton-proton collisions at $\sqrt{s}$ = 13 TeV. *JHEP* (2021) 03:257. doi:10.1007/JHEP03(2021)257

68. Aad G, Abbott B, Abbott D, Abed Abud A, Abeling K, Abhayasinghe D, et al. Combination of searches for Higgs boson pairs in *pp* collisions at $\sqrt{s}$=13 TeV with the ATLAS detector. *Phys Lett B* (2020) 800:135103. doi:10.1016/j.physletb.2019.135103

69. CMS, Tumasyan A, Adam W, Andrejkovic JW, Bergauer T, Chatterjee S, et al. Search for nonresonant Higgs boson pair production in the four leptons plus two b jets final state in proton-proton collisions at $\sqrt{s}$= 13 TeV. *JHEP* (2023). *arXiv* 06:130. doi:10.1007/JHEP06(2023)130

70. CMS, Tumasyan A, Adam W, Andrejkovic JW, Bergauer T, Chatterjee S, et al. Search for Higgs boson pairs decaying to WWWW, WWττ, and ττττ in proton-proton collisions at $\sqrt{s}$= = 13 Te. *JHEP* (2023). *arXiv* 07:095. doi:10.1007/JHEP07(2023)095

71. Cepeda M. Report from working group 2: Higgs physics at the HL-LHC and HE-LHC. *CERN Yellow Rep Monogr* (2019) 7:221–584. doi:10.23731/CYRM-2019-007.221

72. CMS Collaboration. *Prospects for non-resonant Higgs boson pair production measurement in bbγγ final states in proton-proton collisions at $\sqrt{s}$=14 TeV at the High-Luminosity LHC* (2022). *CERN Document Server* [preprint].

73. Abada A, Abbrescia M, AbdusSalam SS, Abdyukhanov I, Abelleira Fernandez J, Abramov A, et al. FCC-ee: The lepton collider: Future circular collider conceptual design report volume 2. *Eur Phys J ST* (2019) 228:261–623. doi:10.1140/epjst/e2019-900045-4

74. Abada A, Abbrescia M, AbdusSalam SS, Abdyukhanov I, Abelleira Fernandez J, Abramov A, et al. FCC-hh: The hadron collider: Future circular collider conceptual design report volume 3. *Eur Phys J ST* (2019) 228:755–1107. doi:10.1140/epjst/e2019-900087-0

75. de Blas J, Cepeda M, D'Hondt J, Ellis R, Grojean C, Heinemann B, et al. Higgs boson studies at future particle colliders. *JHEP* (2020) 01 139. doi:10.1007/jhep01(2020)139

76. Mangano ML, Ortona G, Selvaggi M. Measuring the Higgs self-coupling via Higgs-pair production at a 100 TeV p-p collider. *Eur Phys J C* (2020) 80:1030. doi:10.1140/epjc/s10052-020-08595-3

77. Tinlot J, Green DR. A storage ring for 10 BeV muons. *IEEE Trans Nucl Sci* (1965) 12:470–5. doi:10.1109/TNS.1965.4323677

78. Black KM. *Muon collider forum report* (2022). *arXiv* [preprint].

79. Stratakis D. *A muon collider facility for physics discovery* (2022). *arXiv* [preprint].

80. Chiesa M, Maltoni F, Mantani L, Mele B, Piccinini F, Zhao X. Measuring the quartic Higgs self-coupling at a multi-TeV muon collider. *JHEP* (2020) 09:098. doi:10.1007/JHEP09(2020)098